European Journal of Mechanics / A Solids 111 (2025) 105552

Contents lists available at ScienceDirect

European Journal of Mechanics / A Solids

journal homepage: www.elsevier.com/locate/ejmsol

Full length article

Passive vibration control of a beam modeled through Generalized Beam Theory using a Nonlinear Energy Sink under different loading scenarios

Andrea De Flaviis [a,b,*], Alireza Ture Savadkoohi [b], Daniele Zulli [a]

[a] Department of Civil, Construction-Architectural and Environmental Engineering, University of L'Aquila, Piazzale Pontieri, Loc. Monteluco, L'Aquila, 67100, Italy
[b] ENTPE, École Centrale de Lyon, CNRS, LTDS, UMR5513, Vaulx-en-Velin Cedex, 69518, France

ARTICLE INFO

Keywords:
Nonlinear energy sink
Generalized beam theory
Passive vibration control
Analytical solution

ABSTRACT

In the present paper a beam, part of a box girder bridge, modeled through Generalized Beam Theory is studied. In particular, vibrations are controlled by using a Nonlinear Energy Sink for different types of external loads. The objective is to combine this refined theory, which enables to consider interesting aspects of Thin-Walled Beams, with the concept of vibrations control through nonlinear devices, to take into account real scenarios where the use of classical beam theories and linear dampers could not be sufficient. The fundamental aspects of Generalized Beam Theory are first introduced, identifying its two main phases, cross-section analysis and member analysis, then Complexification Averaging and Multiple Scales Method are used to study the nonlinear problem, where the nonlinearity is represented by the cubic stiffness of the Nonlinear Energy Sink. Different load conditions are investigated, including earthquake and moving loads, and it is found that energy is correctly transferred from the beam to the device and, thanks to Generalized Beam Theory, vibrations due to resonant loads, with frequencies which cannot be found with classical beam theories, can be reduced. It is found that the use of a Nonlinear Energy Sink on a Thin-Walled Beam allows to reduce the vibrations even for complex loading cases, and GBT appears to be a very valuable tool in assessing this aspect. Results obtained in this paper, after proper optimization and experimental validation, could help the implementation of Nonlinear Energy Sinks on real bridge decks.

1. Introduction

Passive vibration control of civil engineering structures is a central and actual topic that involves more and more researchers. Its roots can be found in the pioneering patent of Frahm (1911) which, after its publication, led to the spread of linear devices called Tuned Mass Dampers (TMD) (Den Hartog, 1947; Ioi and Ikeda, 1978; Fujino and Abé, 1993; Wang et al., 2001; Gattulli et al., 2001; Bakre and Jangid, 2007; Casalotti et al., 2014). The TMD is efficient at a narrow frequency width, i.e. around the tuned frequency, but it loses its efficiency elsewhere and moreover its mass can be quite big, which can result in a practical problem. Roberson (1952) has been one of the first to extend the concept of passive vibrations control to nonlinear devices, using a spring with a linear and a cubic term, paving the way to other nonlinear systems. As a consequence, an evolution of those systems started in last two decades, through the use of nonlinear devices, mainly Nonlinear Energy Sinks (NES) especially with cubic nonlinearity (Gendelman et al., 2000, 2008; Gendelman and Starosvetsky, 2006; Starosvetsky and Gendelman, 2008, 2011; Zulli and Luongo, 2016; Vaurigaud et al., 2011). Their main characteristics are the low weight with respect to the main mass and, differently from TMDs, the nonlinear (and nonlinearizable) stiffness, which enables them to control a wide range of frequencies; moreover, as TMDs, they are also equipped with a damper, which enables them to dissipate the energy which is transferred in one way from the main structure to the NES (Vakakis et al., 2008). In the literature, large emphasis has been given to NESs with cubic nonlinearity, but other types of devices, like non-smooth NES, vibro-impact NES, rotary NES, NES with nonlinear damping and others have been considered too (Gourdon and Lamarque, 2005; Lamarque et al., 2011; Ding and Chen, 2020; Saeed et al., 2023; Hurel et al., 2019a,b; Leroux et al., 2023; da Silveira Zanin et al., 2022; Chen et al., 2019). Even if the majority of works focuses on discrete systems, significant contributions about continuous systems can also be found such as for beams and cables (Georgiades and Vakakis, 2007; Zulli and Luongo, 2015; Luongo and Zulli, 2015; Zhang et al., 2020; Wang et al., 2023).

The dynamical behavior of the main structure coupled to the NES can be analytically addressed in different ways: among them, the

* Corresponding author at: Department of Civil, Construction-Architectural and Environmental Engineering, University of L'Aquila, Piazzale Pontieri, Loc. Monteluco, L'Aquila, 67100, Italy.
E-mail address: andrea.deflaviis@graduate.univaq.it (A. De Flaviis).

https://doi.org/10.1016/j.euromechsol.2024.105552
Received 29 August 2024; Received in revised form 30 November 2024; Accepted 22 December 2024
Available online 28 December 2024

most diffused methods are Complexification Averaging (CXA) with Multiple Scales Method (MSM) (Manevitch, 2001; Nayfeh and Mook, 1995; Ture Savadkoohi et al., 2016) and the Multiple Scales/Harmonic Balance Method (MSHBM) (Luongo and Zulli, 2012, 2014).

In this work, the main structure to be controlled by the NES is a beam, which is modeled through Generalized Beam Theory (GBT), an analytical formulation specifically developed to solve problems related to Thin-Walled Beams (TWB), to take into account fundamental aspects, e.g. the deformation of the cross-section in its own plane and out-of plane. The primordial idea is traced back to the work of Schardt in 1966 (Schardt, 1966), but a great impulse was given in 90's with his contribute and that of other authors among which Schardt (1994) and Davies and Leach (1992, 1994). Since then, works based on GBT rapidly grew up in number, facing a wide spectrum of problems: see Silvestre and Camotim (2002, 2003), Bebiano et al. (2015), Camotim et al. (2008) and Gonçalves et al. (2023) and related bibliography. In the meanwhile, Ranzi and Luongo (2011) and Piccardo et al. (2013) developed an alternative procedure to perform the first phase of GBT, namely the cross-section analysis, proposing the so called GBT-D. It has been used by the authors in De Flaviis et al. (2024) to compare the static and free dynamic responses of a beam modeled through GBT with the ones obtained from experimental results, showing that the model is able to capture the real beam behaviors. Moreover, in that work an Euler–Bernoulli model has been used too, highlighting that it cannot correctly predict the behavior of the box-girder beam, even for static loads.

The use of GBT in this work is motivated by the shape of the beam cross-section and by the necessity of considering different types of loads with different frequencies, which can excite certain vibration modes having torsional or local nature, that cannot be identified with simple beam theories like Euler–Bernoulli or Timoshenko ones. In addition, a classical beam theory cannot take into account the deformation of the cross-section in and out-of plane which can be a crucial aspect for some load cases.

On the other side, it is shown that using a nonlinear device like a NES for vibration control, rather than a linear one, vibrations amplitude can be effectively reduced in a wide range of frequencies, with the same NES in a very effective way.

The paper is organized as follows. In Section 2 the fundamental concepts of GBT are introduced with main equations, then in Section 3 the NES is added and the nonlinear problem is explained in detail at fast and slow time scales. In Section 4 different types of loads are introduced and in Section 5 results are reported. Conclusions and future perspectives are resumed in Section 6.

2. Analytical model

The system under analysis is constituted by a simply supported elastic beam having initial length L and boxed cross-section (see Fig. 1). It is representative of the generic span of a simply supported bridge, where the deformation effect of the pillars is assumed negligible and the spans are independent. The model tries to portray a real existing pre-stressed reinforced concrete beam despite some hypotheses made in the modelization and in the choice of some parameters.

A brief description of modeling according to the GBT-D technique is given here, while more details can be found in Ranzi and Luongo (2011) and Piccardo et al. (2013). The displacement field is written as a linear combination of pre-determined "deformation modes" of the cross-section, depending on its curvilinear abscissa, and unknown "amplitude functions", depending on the axial coordinate and time. In this way a TWB can be studied in a simplified manner, without losing its typical features.

GBT is made of two main phases: (i) the cross-section analysis, which is the distinctive feature of the procedure, where the deformation modes are determined (more details can be found in Section 2.1) and (ii) the member-analysis, where the equilibrium equations are solved with respect to the amplitude functions, thus getting the displacement

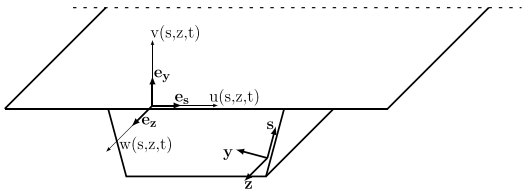

Fig. 1. Cross-section with displacement field.

field of the beam (more details can be found in Section 2.2). Both of these phases are essential: the first one to correctly model the deformation of the cross-section, the second one to solve the problem, thus finding the solution. Deformation modes can be classified in accordance with GBT-D as: (i) conventional: with the Vlasov's hypotheses of membrane inextensibility in the tangential direction and membrane shear indeformability (among these modes another subdivision can be made into rigid, distortional and local), (ii) extensional: where the hypothesis of membrane inextensibility is released and (iii) shear or warping: particularly important for short beams.

With reference to Fig. 1, s, y and z are the tangential, transversal and axial coordinate of every element making up the section, and $u(s,z,t)$, $v(s,z,t)$ and $w(s,z,t)$ are the displacement components in the respective directions. Using the aforementioned combination of conventional deformation modes $\mathbf{U}(s)$, $\mathbf{V}(s)$ and $\mathbf{\Omega}(s)$ (the first two terms are non-dimensional, the third has dimension of a length) with amplitude functions $\boldsymbol{\varphi}(z,t)$ (with dimension of a length), the displacement field is the following (all previous are n_d column vector functions, where n_d is the number of chosen deformation modes):

$$\begin{cases} u(s,z,t) = \mathbf{U}^T(s)\boldsymbol{\varphi}(z,t) \\ v(s,z,t) = \mathbf{V}^T(s)\boldsymbol{\varphi}(z,t) \\ w(s,z,t) = \mathbf{\Omega}^T(s)\boldsymbol{\varphi}'(z,t) \end{cases} \tag{1}$$

where the first derivative on $\boldsymbol{\varphi}(z,t)$ with respect to z (indicated by the prime) is due to the hypothesis of membrane shear indeformability. Then, the strain field (with axial ε and shear γ strain measures), with membrane (superscript m) and flexural (superscript f) components, is written as:

$$\begin{pmatrix} \varepsilon_s^m \\ \varepsilon_z^m \\ \gamma_{zs}^m \\ \varepsilon_s^f \\ \varepsilon_z^f \\ \gamma_{zs}^f \end{pmatrix} = \begin{pmatrix} u_{,s} \\ w_{,z} \\ u_{,z} + w_{,s} \\ -yv_{,ss} \\ -yv_{,zz} \\ -2yv_{,sz} \end{pmatrix} = \begin{pmatrix} \mathbf{U}'^T\boldsymbol{\varphi} \\ \mathbf{\Omega}^T\boldsymbol{\varphi}'' \\ (\mathbf{U}^T + \mathbf{\Omega}'^T)\boldsymbol{\varphi}' \\ -y\mathbf{V}''^T\boldsymbol{\varphi} \\ -y\mathbf{V}^T\boldsymbol{\varphi}'' \\ -2y\mathbf{V}'^T\boldsymbol{\varphi}' \end{pmatrix} \tag{2}$$

Considering a linear elastic behavior, the active plane stress vector is written as follows, where E is Young modulus, G is shear modulus, ν is Poisson's ratio, σ and τ are the axial and shear stress respectively.

$$\begin{pmatrix} \sigma_s^m \\ \sigma_z^m \\ \tau_{zs}^m \\ \sigma_s^f \\ \sigma_z^f \\ \tau_{zs}^f \end{pmatrix} = \begin{bmatrix} E & 0 & 0 & 0 & 0 & 0 \\ 0 & E & 0 & 0 & 0 & 0 \\ 0 & 0 & G & 0 & 0 & 0 \\ 0 & 0 & 0 & \dfrac{E}{1-\nu^2} & \dfrac{\nu E}{1-\nu^2} & 0 \\ 0 & 0 & 0 & \dfrac{\nu E}{1-\nu^2} & \dfrac{E}{1-\nu^2} & 0 \\ 0 & 0 & 0 & 0 & 0 & G \end{bmatrix} \begin{pmatrix} \varepsilon_s^m \\ \varepsilon_z^m \\ \gamma_{zs}^m \\ \varepsilon_s^f \\ \varepsilon_z^f \\ \gamma_{zs}^f \end{pmatrix} \tag{3}$$

Since only conventional deformation modes are kept, $\varepsilon_s^m = 0$ and $\gamma_{zs}^m = 0$ or $\gamma_{zs}^m = const$ on closed loops. Using Hamilton's Principle, in the general dynamical case, the following equilibrium equation with boundary conditions is obtained:

$$\mathbf{M}\ddot{\boldsymbol{\varphi}}(z,t) - \mathbf{Q}_{\Omega\Omega}^M\ddot{\boldsymbol{\varphi}}''(z,t) + (\mathbf{C}^f + \mathbf{C}_{\Omega\Omega}^a)\boldsymbol{\varphi}''''(z,t)$$

$$+ (\mathbf{D}^f + \mathbf{D}^{fT} - \mathbf{D}^s_{\Omega\Omega} - \mathbf{D}^t)\boldsymbol{\varphi}''(z,t) + \mathbf{B}^f\boldsymbol{\varphi}(z,t) = \mathbf{p}_\Omega(z,t) \tag{4}$$

$$\delta\boldsymbol{\varphi}'^T(z,t)[(\mathbf{C}^f + \mathbf{C}^a_{\Omega\Omega})\boldsymbol{\varphi}''(z,t) + \mathbf{D}^f\boldsymbol{\varphi}(z,t)]|_0^L = 0 \quad \forall t \tag{5}$$

$$\delta\boldsymbol{\varphi}^T(z,t)[-\mathbf{Q}^M_{\Omega\Omega}\ddot{\boldsymbol{\varphi}}'(z,t) + (\mathbf{C}^f + \mathbf{C}^a_{\Omega\Omega})\boldsymbol{\varphi}'''(z,t) + (\mathbf{D}^f - \mathbf{D}^s_{\Omega\Omega} - \mathbf{D}^t)\boldsymbol{\varphi}'(z,t)]|_0^L = 0 \quad \forall t \tag{6}$$

where δ indicates first variation and dot stands for time derivative. The symmetric $n_d \times n_d$ mass and stiffness matrices ($\mathbf{M}$, $\mathbf{Q}^M_{\Omega\Omega}$, $\mathbf{C}^f$, ...) written in Eqs. (4)–(6) are defined below, where m is mass per unit area and h is thickness along y. Moreover, $\mathbf{p}_\Omega$ is the load vector in the general case of forces per unit area applied in all three directions:

$$\mathbf{M} = \int_S m(\mathbf{U}\mathbf{U}^T + \mathbf{V}\mathbf{V}^T)ds, \qquad \mathbf{Q}^M_{\Omega\Omega} = \int_S m\boldsymbol{\Omega}\boldsymbol{\Omega}^T ds \tag{7}$$

$$\mathbf{C}^f = \int_S \frac{Eh^3}{12(1-\nu^2)}\mathbf{V}\mathbf{V}^T ds, \qquad \mathbf{C}^a_{\Omega\Omega} = \int_S Eh\boldsymbol{\Omega}\boldsymbol{\Omega}^T ds \tag{8}$$

$$\mathbf{D}^s_{\Omega\Omega} = \int_S Gh(\boldsymbol{\Omega}'^T + \mathbf{U}^T)^T(\boldsymbol{\Omega}'^T + \mathbf{U}^T)ds \tag{9}$$

$$\mathbf{D}^f = \int_S \frac{\nu Eh^3}{12(1-\nu^2)}\mathbf{V}\mathbf{V}''^T ds, \quad \mathbf{D}^t = \int_S \frac{Gh^3}{3}\mathbf{V}'\mathbf{V}'^T ds \tag{10}$$

$$\mathbf{B}^f = \int_S \frac{Eh^3}{12(1-\nu^2)}\mathbf{V}''\mathbf{V}''^T ds \tag{11}$$

$$\mathbf{p}_\Omega = \int_S \left(f_s\mathbf{U} + f_y\mathbf{V} - f'_z\boldsymbol{\Omega}\right) ds \tag{12}$$

where the integrals are evaluated in the cross-section domain S.

2.1. Cross-section analysis

Cross-section analysis is a crucial step of GBT, as it involves the determination of deformation modes of the cross-section which affects the quality of the response. A full detailed explanation of how it is performed in the framework of GBT-D can be found in Piccardo et al. (2013); main features are here resumed. Basically, to find conventional modes, the free dynamics problem of the externally unrestrained cross-section (in the plane orthogonal to z) has to be studied, which implies, in the order, the following steps:

(i) The cross-section is discretized in finite elements (FE) by introducing intermediate nodes, each of which has 3 degrees of freedom (two translations and one rotation). The classical stiffness and mass matrices of each element are built and then assembled to get those of the entire cross-section.
(ii) The internal restraint of membrane inextensibility is applied and the dynamical eigenvalue problem with reduced matrices is solved. Since no external restraint exists, 3 zero eigenvalues are found as well, and the corresponding eigenvectors (nodal dofs) represent rigid modes (two translation and one rotation in the plane). The tangential and transversal components of deformation modes $\mathbf{U}(s)$ and $\mathbf{V}(s)$ are obtained from nodal displacements through linear and cubic interpolation functions, respectively.
(iii) Making use of membrane shear indeformability hypothesis, the longitudinal components of deformation modes $\boldsymbol{\Omega}(s)$ are also found, directly related to $\mathbf{U}(s)$. To get the complete set of conventional deformation modes, a fourth rigid mode, representing translation along z, has to be added (this is normally obtained as the first of shear or warping modes, not considered in this work).

Some of cross-section deformation modes are shown in Fig. 2 in terms of displacements in the plane of the cross-section (labeled as $\mathbf{U}(s)$, $\mathbf{V}(s)$) and along the beam axis (labeled as $\boldsymbol{\Omega}(s)$).

2.2. Member analysis

Member analysis, i.e. resolution of equilibrium Eqs. (4)–(6) to find the unknowns $\boldsymbol{\varphi}(z,t)$ can be performed either analytically or numerically, e.g. using finite elements for the latter. In the case of a simply supported beam, as in the present work, it has been shown in Bebiano et al. (2013) that an analytical solution is possible, both for free and forced dynamics. The analytical solution in free dynamics, i.e. natural frequencies and vibration modes, is here resumed, since it will be used in the following. Considering the jth vibration mode, free dynamics equation with boundary conditions representing simply supported beam, derived from Eqs. (4)–(6), are:

$$\mathbf{M}\ddot{\boldsymbol{\varphi}}_j(z,t) - \mathbf{Q}^M_{\Omega\Omega}\ddot{\boldsymbol{\varphi}}''_j(z,t) + (\mathbf{C}^f + \mathbf{C}^a_{\Omega\Omega})\boldsymbol{\varphi}''''_j(z,t) + (\mathbf{D}^f + \mathbf{D}^{fT} - \mathbf{D}^s_{\Omega\Omega} - \mathbf{D}^t)\boldsymbol{\varphi}''_j(z,t) + \mathbf{B}^f\boldsymbol{\varphi}_j(z,t) = \mathbf{0} \tag{13}$$

$$[(\mathbf{C}^f + \mathbf{C}^a_{\Omega\Omega})\boldsymbol{\varphi}''_j(z,t) + \mathbf{D}^f\boldsymbol{\varphi}_j(z,t)]|_0^L = \mathbf{0} \quad \forall t \tag{14}$$

$$\boldsymbol{\varphi}_j(z,t)|_0^L = \mathbf{0} \quad \forall t \tag{15}$$

where the jth amplitude function can be written separating space and time as:

$$\boldsymbol{\varphi}_j(z,t) = \boldsymbol{\Phi}_j(z)Y_j(t) \tag{16}$$

where $\boldsymbol{\Phi}_j(z)$ is the column vector of dimension n_d representing the jth vibration mode, while $Y_j(t)$ is the modal coordinate. As a consequence, Eq. (13) can be split into the following (ω_j being the jth angular frequency in rad/s):

$$\ddot{Y}_j(t) + \omega_j^2 Y_j(t) = 0 \tag{17}$$

$$(\mathbf{C}^f + \mathbf{C}^a_{\Omega\Omega})\boldsymbol{\Phi}''''_j(z) + (\mathbf{D}^f + \mathbf{D}^{fT} - \mathbf{D}^s_{\Omega\Omega} - \mathbf{D}^t)\boldsymbol{\Phi}''_j(z) + \mathbf{B}^f\boldsymbol{\Phi}_j(z) - \omega_j^2\left(\mathbf{M}\boldsymbol{\Phi}_j(z) - \mathbf{Q}^M_{\Omega\Omega}\boldsymbol{\Phi}''_j(z)\right) = \mathbf{0} \tag{18}$$

The goal is to analytically solve Eq. (18) to find natural frequencies and vibration modes. To do that, it can be observed that a solution that satisfies boundary conditions (5), (6) is:

$$\boldsymbol{\Phi}_j(z) = \boldsymbol{\Theta}_j \sin\left(\frac{n_j\pi z}{L}\right) \tag{19}$$

where $\boldsymbol{\Theta}_j$ and n_j are the magnitude and the longitudinal half-wave number of the jth vibration mode, respectively. The magnitudes, as well as the squared angular frequencies ω_j^2, are determined substituting Eq. (19) into Eq. (18), thus obtaining a problem like:

$$\left(\mathbf{K}_j - \omega_j^2\mathbf{M}_j\right)\boldsymbol{\Theta}_j = \mathbf{0} \tag{20}$$

where the stiffness and mass matrices are:

$$\mathbf{K}_j = (\mathbf{C}^f + \mathbf{C}^a_{\Omega\Omega})\left(\frac{n_j\pi}{L}\right)^4 - (\mathbf{D}^f + \mathbf{D}^{fT} - \mathbf{D}^s_{\Omega\Omega} - \mathbf{D}^t)\left(\frac{n_j\pi}{L}\right)^2 + \mathbf{B}^f \tag{21}$$

$$\mathbf{M}_j = \mathbf{M} + \mathbf{Q}^M_{\Omega\Omega}\left(\frac{n_j\pi}{L}\right)^2 \tag{22}$$

Solving the eigenvalue problem (20), the total number of vibration modes is $n_v = n_d \times N_j$ with N_j maximum half-wave number considered; some of them are showed in Fig. 3.

It can be proved, following classical steps (projection on a generic vibration mode $\boldsymbol{\Phi}_h(z)$), that orthogonality with respect to the mass and stiffness operators exists among all found vibration modes. This means that, in the generic case where a dynamical force acts on the beam, uncoupled equations can be solved for every vibration mode and their contribution summed, retaining only a limited number of modes:

$$\boldsymbol{\varphi}(z,t) = \sum_{j=1}^{n_v}\boldsymbol{\Phi}_j(z)Y_j(t) = \boldsymbol{\Phi}(z)\mathbf{Y}(t) \tag{23}$$

where $\boldsymbol{\Phi}(z)$ is a $n_d \times n_v$ matrix function where each row corresponds to a deformation mode and each column to a vibration mode, while $\mathbf{Y}(t)$ is

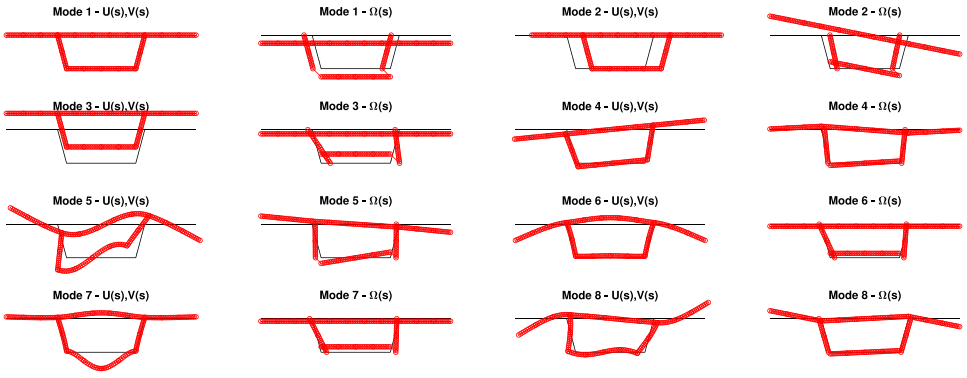

Fig. 2. First conventional deformation modes with in-plane and out-of plane components.

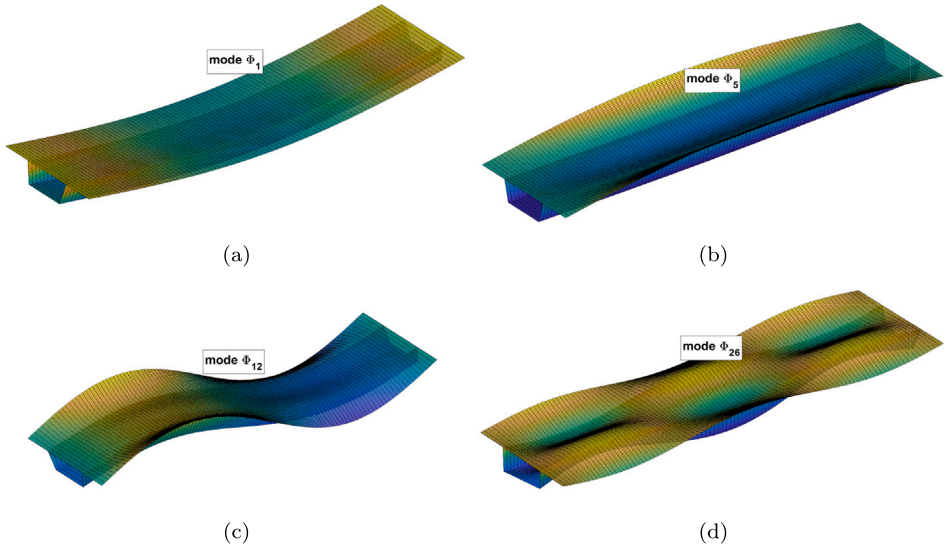

Fig. 3. Some of the n_v vibration modes. (a) $n_j = 1$: Φ_1, (b) $n_j = 1$: Φ_5; (c) $n_j = 2$: Φ_{12}; (d) $n_j = 3$: Φ_{26}.

a n_v column vector function, where each row is the time response of a vibration mode to a given load. As a consequence, substituting Eq. (23) inside Eq. (1), the transversal displacement becomes:

$$v(s,z,t) = \mathbf{V}^T(s)\boldsymbol{\Phi}(z)\mathbf{Y}(t)$$
$$= \begin{pmatrix} V_1(s) & \dots & V_{n_d}(s) \end{pmatrix} \begin{bmatrix} \boldsymbol{\Phi}_{11}(z) & \dots & \boldsymbol{\Phi}_{1n_v}(z) \\ \vdots & \ddots & \vdots \\ \boldsymbol{\Phi}_{n_d1}(z) & \dots & \boldsymbol{\Phi}_{n_dn_v}(z) \end{bmatrix} \begin{pmatrix} Y_1(t) \\ \vdots \\ Y_{n_v}(t) \end{pmatrix} \tag{24}$$

This representation emphasizes the difference between deformation modes and vibration modes and highlights the possibility to choose an arbitrary number of each of them.

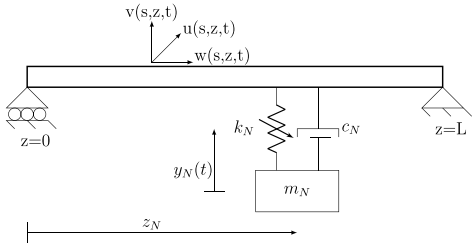

Fig. 4. Scheme of the beam coupled with NES.

3. Nonlinear problem

In this Section, a NES is added to the beam, with the objective of controlling vibrations due to different types of loads.

3.1. Formulation

The NES is shown in Fig. 4 together with a sketch of the simply supported beam representing the longitudinal direction of the bridge, where m_N, k_N and c_N are the mass, cubic stiffness and damping of the NES respectively, z_N being its position along the beam axis and $y_N(t)$ its absolute vertical displacement.

Equilibrium equations of the undamped beam with the attached NES can be written as follows, where all symbols have been explained before:

$$\mathbf{M}\ddot{\boldsymbol{\varphi}}(z,t) - \mathbf{Q}^M_{\Omega\Omega}\ddot{\boldsymbol{\varphi}}''(z,t) + (\mathbf{C}^f + \mathbf{C}^a_{\Omega\Omega})\boldsymbol{\varphi}''''(z,t)$$
$$+ (\mathbf{D}^f + \mathbf{D}^{fT} - \mathbf{D}^s_{\Omega\Omega} - \mathbf{D}^t)\boldsymbol{\varphi}''(z,t) + \mathbf{B}^f\boldsymbol{\varphi}(z,t)$$
$$+ \mathbf{V}(s_N)[k_N(\mathbf{V}^T(s_N)\boldsymbol{\varphi}(z,t) - y_N(t))^3$$
$$+ c_N(\mathbf{V}^T(s_N)\dot{\boldsymbol{\varphi}}(z,t) - \dot{y}_N(t))]\delta(z - z_N) = \mathbf{p}_\Omega(z,t) \tag{25}$$

$$m_N\ddot{y}_N(t) - [k_N(\mathbf{V}^T(s_N)\boldsymbol{\varphi}(z_N,t) - y_N(t))^3$$
$$+ c_N(\mathbf{V}^T(s_N)\dot{\boldsymbol{\varphi}}(z_N,t) - \dot{y}_N(t))] = 0 \tag{26}$$

where $\delta(z - z_N)$ is the Dirac function, which provides the position of the NES along the beam. Since the goal is to study a 1:1 resonance

and internal resonances are not considered, it can be assumed that the response of the system is dominated by its jth vibration mode, i.e. $\boldsymbol{\varphi}(z,t) = \boldsymbol{\Phi}_j(z)Y_j(t)$ and Eq. (25) is projected on it. Furthermore, at this point damping is added to the beam as $C_j = 2\xi_j M_j \omega_j$ where ξ_j is modal damping coefficient.

$$\begin{aligned} &M_j\ddot{Y}_j(t) + C_j\dot{Y}_j(t) + K_jY_j(t) \\ &+ \boldsymbol{\Phi}_j^T(z_N)\mathbf{V}(s_N)[k_N(\mathbf{V}^T(s_N)\boldsymbol{\Phi}_j(z_N)Y_j(t) - y_N(t))^3 \\ &+ c_N(\mathbf{V}^T(s_N)\boldsymbol{\Phi}_j(z_N)\dot{Y}_j(t) - \dot{y}_N(t))] = \int_0^L \boldsymbol{\Phi}_j^T(z)\mathbf{p}_\Omega(z,t)dz \end{aligned} \tag{27}$$

$$\begin{aligned} &m_N\ddot{y}_N(t) - [k_N(\mathbf{V}^T(s_N)\boldsymbol{\Phi}_j(z_N)Y_j(t) - y_N(t))^3 \\ &+ c_N(\mathbf{V}^T(s_N)\boldsymbol{\Phi}_j(z_N)\dot{Y}_j(t) - \dot{y}_N(t))] = 0 \end{aligned} \tag{28}$$

where mass and stiffness terms are:

$$M_j = \int_0^L \boldsymbol{\Phi}_j^T(z)[\mathbf{M}\boldsymbol{\Phi}_j(z) - \mathbf{Q}^M_{\Omega\Omega}\boldsymbol{\Phi}_j''(z)]dz \tag{29}$$

$$\begin{aligned} K_j = &\int_0^L \boldsymbol{\Phi}_j^T(z)[(\mathbf{C}^f + \mathbf{C}^a_{\Omega\Omega})\boldsymbol{\Phi}_j''''(z) \\ &+ (\mathbf{D}^f + \mathbf{D}^{fT} - \mathbf{D}^s_{\Omega\Omega} - \mathbf{D}^t)\boldsymbol{\Phi}_j''(z) + \mathbf{B}^f\boldsymbol{\Phi}_j(z)]dz \end{aligned} \tag{30}$$

Non-dimensional parameters are introduced as follows:

$$\tilde{z} = \frac{z}{b_1}, \qquad \tau = \omega_j t, \qquad \tilde{y}_N(\tau) = \frac{y_N(t)}{b_1} \tag{31}$$

$$\varepsilon\tilde{k}_N = \frac{k_N b_1^2}{K_j}, \qquad \varepsilon\tilde{c}_N = \frac{c_N\omega_j}{K_j}, \qquad \varepsilon\hat{C}_j = 2\xi_j \tag{32}$$

$$\tilde{\mathbf{V}}(\tilde{s}_N) = \mathbf{V}(s_N), \qquad \tilde{\boldsymbol{\Phi}}_j(\tilde{z}_N) = \boldsymbol{\Phi}_j(z_N), \qquad \tilde{Y}_j(\tau) = \frac{Y_j(t)}{b_1} \tag{33}$$

$$\varepsilon\Gamma = \frac{1}{M_j\omega_j^2 b_1}\int_0^L \boldsymbol{\Phi}_j^T(z)\mathbf{p}_\Omega(z,t)dz \tag{34}$$

where b_1 is a characteristic length of the beam and ε is a small non-dimensional parameter accounting for the ratio between the mass of the NES and that of the beam to be controlled as:

$$0 < \varepsilon = \frac{m_N}{M_j} \ll 1 \tag{35}$$

Putting non-dimensional variables into Eqs. (27)–(28), they become the following, where $\dot{()} = d/d\tau$:

$$\begin{aligned} &\ddot{\tilde{Y}}_j(\tau) + \varepsilon\hat{C}_j\dot{\tilde{Y}}_j(\tau) + \tilde{Y}_j(\tau) \\ &+ \tilde{\boldsymbol{\Phi}}_j^T(\tilde{z}_N)\tilde{\mathbf{V}}(\tilde{s}_N)[\varepsilon\tilde{k}_N(\tilde{\mathbf{V}}^T(\tilde{s}_N)\tilde{\boldsymbol{\Phi}}_j(\tilde{z}_N)\tilde{Y}_j(\tau) - \tilde{y}_N(\tau))^3 \\ &+ \varepsilon\tilde{c}_N(\tilde{\mathbf{V}}^T(\tilde{s}_N)\tilde{\boldsymbol{\Phi}}_j(\tilde{z}_N)\dot{\tilde{Y}}_j(\tau) - \dot{\tilde{y}}_N(\tau))] = \varepsilon\Gamma \end{aligned} \tag{36}$$

$$\begin{aligned} &\varepsilon\ddot{\tilde{y}}_N(\tau) - [\varepsilon\tilde{k}_N(\tilde{\mathbf{V}}^T(\tilde{s}_N)\tilde{\boldsymbol{\Phi}}_j(\tilde{z}_N)\tilde{Y}_j(\tau) - \tilde{y}_N(\tau))^3 \\ &+ \varepsilon\tilde{c}_N(\tilde{\mathbf{V}}^T(\tilde{s}_N)\tilde{\boldsymbol{\Phi}}_j(\tilde{z}_N)\dot{\tilde{Y}}_j(\tau) - \dot{\tilde{y}}_N(\tau))] = 0 \end{aligned} \tag{37}$$

Equations are rearranged introducing new variables representing the relative displacement a between the beam and the NES, in the point where the NES is attached, and a quantity r which represents the displacement of the center of mass of the coupled system as:

$$\begin{pmatrix} a \\ r \end{pmatrix} = \begin{bmatrix} \tilde{\mathbf{V}}^T(\tilde{s}_N)\tilde{\boldsymbol{\Phi}}_j(\tilde{z}_N) & -1 \\ 1 & \varepsilon \end{bmatrix} \begin{pmatrix} \tilde{Y}_j \\ \tilde{y}_N \end{pmatrix} \tag{38}$$

So, equilibrium equations are rewritten, with $\chi_j = \tilde{\boldsymbol{\Phi}}_j^T(\tilde{z}_N)\tilde{\mathbf{V}}(\tilde{s}_N)$ and $D = 1 + \varepsilon\chi_j$, as:

$$\begin{aligned} &\ddot{r} + \frac{\varepsilon\hat{C}_j}{D}(\varepsilon\dot{a} + \dot{r}) + \frac{1}{D}(\varepsilon a + r) + \varepsilon\tilde{k}_N\left(\chi_j - 1\right)a^3 \\ &+ \varepsilon\tilde{c}_N\left(\chi_j - 1\right)\dot{a} = \varepsilon\Gamma \end{aligned} \tag{39}$$

$$\begin{aligned} &\ddot{a} + \frac{\varepsilon\chi_j\hat{C}_j}{D}(\varepsilon\dot{a} + \dot{r}) + \frac{\chi_j}{D}(\varepsilon a + r) + \tilde{k}_N\left(\varepsilon\chi_j^2 + 1\right)a^3 \\ &+ \tilde{c}_N\left(\varepsilon\chi_j^2 + 1\right)\dot{a} = \varepsilon\chi_j\Gamma \end{aligned} \tag{40}$$

In the spirit of the Complexification Averaging Method, complex variables β_1, β_2 by Manevitch (2001) are introduced (i is the imaginary unit):

$$\begin{cases} \beta_1 e^{i\Omega\tau} = \dot{r} + i\Omega r \\ \beta_2 e^{i\Omega\tau} = \dot{a} + i\Omega a \end{cases} \tag{41}$$

At this point, since the goal is to solve the problem through Multiple Scales Method (Nayfeh and Mook, 1995), different time scales are introduced and complex variables are rewritten as:

$$\beta_j(\tau) = \beta_j(\tau_0, \tau_1, \ldots), \quad \tau_i = \varepsilon^i\tau, \qquad i = 1,2 \tag{42}$$

and applying Galerkin's method, using $()^*$ to denote complex conjugate of a variable, only harmonic of frequency Ω is kept, i.e.:

$$x(\beta_1, \beta_2, \beta_1^*, \beta_2^*) = \frac{\Omega}{2\pi}\int_0^{\frac{2\pi}{\Omega}} X(\beta_1, \beta_2, \beta_1^*, \beta_2^*)e^{-i\Omega\tau}d\tau \tag{43}$$

The hypothesis, to be proved, is that variables β_j do not depend on the fast time scale $\tau_0 = \tau$ (or system will be studied at the infinity of fast time scale, i.e. for $\tau_0 \to \infty$). As a consequence, equilibrium equations are finally rewritten as:

$$\begin{aligned} &\dot{\beta}_1 + \frac{i\Omega}{2}\beta_1 + \frac{\varepsilon\hat{C}_j}{2D}(\beta_1 + \varepsilon\beta_2) + \frac{1}{2i\Omega D}(\beta_1 + \varepsilon\beta_2) \\ &+ \frac{3}{8i\Omega^3}\varepsilon\tilde{k}_N\left(\chi_j - 1\right)\beta_2^2\beta_2^* + \frac{1}{2}\varepsilon\tilde{c}_N\left(\chi_j - 1\right)\beta_2 \\ &= \frac{\Omega}{2\pi}\int_0^{\frac{2\pi}{\Omega}} \varepsilon\Gamma e^{-i\Omega\tau}d\tau \end{aligned} \tag{44}$$

$$\begin{aligned} &\dot{\beta}_2 + \frac{i\Omega}{2}\beta_2 + \frac{\varepsilon\chi_j\hat{C}_j}{2D}(\beta_1 + \varepsilon\beta_2) + \frac{\chi_j}{2i\Omega D}(\beta_1 + \varepsilon\beta_2) \\ &+ \frac{3}{8i\Omega^3}\tilde{k}_N\left(\varepsilon\chi_j^2 + 1\right)\beta_2^2\beta_2^* + \frac{1}{2}\tilde{c}_N\left(\varepsilon\chi_j^2 + 1\right)\beta_2 \\ &= \frac{\Omega}{2\pi}\int_0^{\frac{2\pi}{\Omega}} \varepsilon\chi_j\Gamma e^{-i\Omega\tau}d\tau \end{aligned} \tag{45}$$

where the derivative with respect to non-dimensional time is:

$$\frac{d(..)}{d\tau} = \frac{\partial(...)}{\partial\tau_0} + \varepsilon\frac{\partial(...)}{\partial\tau_1} + \varepsilon^2\frac{\partial(...)}{\partial\tau_2} + \cdots = d_0 + \varepsilon d_1 + \varepsilon^2 d_2 + \cdots \tag{46}$$

As a consequence of the introduction of multiple scales, the system behavior is studied at different orders of ε, i.e. at different scales of time, with the higher orders ε being corrections to the lower order ones. Moreover, to study the system around a 1:1 resonance, it should be set:

$$\Omega = \Omega_F/\omega_j = 1 + \varepsilon\sigma \tag{47}$$

where Ω_F is the angular frequency of the external load and σ is a detuning parameter that permits to study the system near the resonance. Collecting all terms at the same order of ε until ε^1 leads to:

$$\text{order } \varepsilon^0 : \; d_0\beta_1 + \frac{i}{2}\beta_1 + \frac{1}{2iD}\beta_1 = 0 \tag{48}$$

$$d_0\beta_2 + \frac{i}{2}\beta_2 + \frac{\chi_j}{2iD}\beta_1 + \frac{3}{8i}\tilde{k}_N\beta_2^2\beta_2^* + \frac{1}{2}\tilde{c}_N\beta_2 = 0 \tag{49}$$

$$\begin{aligned} &\text{order } \varepsilon^1 : \; d_1\beta_1 + \frac{i\sigma}{2}\beta_1 + \frac{\hat{C}_j}{2D}\beta_1 + \frac{1}{2iD}(\beta_2 - \sigma\beta_1) \\ &+ \frac{3}{8i}\tilde{k}_N\left(\chi_j - 1\right)\beta_2^2\beta_2^* + \frac{1}{2}\tilde{c}_N\left(\chi_j - 1\right)\beta_2 = \frac{\Omega}{2\pi}\int_0^{\frac{2\pi}{\Omega}} \Gamma e^{-i\Omega\tau}d\tau \end{aligned} \tag{50}$$

$$\begin{aligned} &d_1\beta_2 + \frac{i\sigma}{2}\beta_2 + \frac{\chi_j\hat{C}_j}{2D}\beta_1 + \frac{\chi_j}{2iD}(\beta_2 - \sigma\beta_1) \\ &+ \frac{3}{8i}\tilde{k}_N\left(\chi_j^2 - 3\sigma\right)\beta_2^2\beta_2^* + \frac{1}{2}\tilde{c}_N\chi_j^2\beta_2 = \frac{\Omega}{2\pi}\int_0^{\frac{2\pi}{\Omega}} \chi_j\Gamma e^{-i\Omega\tau}d\tau \end{aligned} \tag{51}$$

3.2. Fast time scale

Starting from Eq. (48), since $D \approx 1$, it results that $d_0\beta_1 = 0$, which means that β_1 is independent of fast time τ_0 in accordance to the hypothesis made before. About Eq. (49), an asymptotic state is searched for $\tau_0 \to \infty$, so that $d_0\beta_2 = 0$: this means finding the equilibrium (fixed) points of the system. Doing that, the following equation is obtained:

$$\mathbb{S}(\beta_1, \beta_2, \beta_1^*, \beta_2^*) = \frac{\chi_j}{2i}\beta_1 - \frac{1}{2i}\beta_2 + \frac{3}{8i}\tilde{k}_N\beta_2^2\beta_2^* + \frac{1}{2}\tilde{c}_N\beta_2 = 0 \tag{52}$$

This is the equation of the Slow Invariant Manifold (SIM), a topological manifold, invariant under the action of a dynamical system (Troger and Steindl, 1991; Carr, 1981). To study it, complex variables are written in polar form as:

$$\beta_j = N_j e^{i\delta_j}, \quad j = 1, 2 \tag{53}$$

where $N_j \in \mathbb{R}^+$, $\delta_j \in \mathbb{R}$. Putting Eq. (53) into Eq. (52), the SIM in the real domain is obtained, thus finding the searched equilibrium points:

$$N_1 = \frac{N_2}{\chi_j}\sqrt{\tilde{c}_N^2 + \left(1 - \frac{3}{4}\tilde{k}_N N_2^2\right)^2} \tag{54}$$

To trace stable and unstable zones of the SIM, a small linear perturbation $|\Delta\beta_2| \ll |\beta_2|$ is applied to β_2, i.e. $\beta_2 \to \beta_2 + \Delta\beta_2$ and the same to its complex conjugate. The real part of the eigenvalues of the resulting matrix is studied: if it is negative, the equilibrium points are classified as stable, otherwise they are unstable. After neglecting higher order terms, equation becomes:

$$\begin{pmatrix} \frac{\delta\Delta\beta_2}{\delta\tau_0} \\ \frac{\delta\Delta\beta_2^*}{\delta\tau_0} \end{pmatrix} = \mathbf{A}\begin{pmatrix} \Delta\beta_2 \\ \Delta\beta_2^* \end{pmatrix} \tag{55}$$

where the matrix $\mathbf{A}$ is:

$$\mathbf{A} = \begin{bmatrix} \frac{1}{2i} - \frac{3}{4i}\tilde{k}_N\beta_2\beta_2^* - \frac{1}{2}\tilde{c}_N & -\frac{3}{8i}\tilde{k}_N\beta_2^2 \\ \frac{3}{8i}\tilde{k}_N\beta_2^{*2} & -\frac{1}{2i} + \frac{3}{4i}\tilde{k}_N\beta_2\beta_2^* - \frac{1}{2}\tilde{c}_N \end{bmatrix} \tag{56}$$

The eigenvalues of $\mathbf{A}$ verify the following characteristic polynomial:

$$\lambda^2 - \left(A_{11} + A_{22}\right)\lambda + A_{11}A_{22} - A_{12}A_{21} = 0 \tag{57}$$

It can be observed that following relations exist:

$$\begin{cases} \lambda_1 + \lambda_2 = A_{11} + A_{22} = -\tilde{c}_N < 0 \\ \lambda_1\lambda_2 = A_{11}A_{22} - A_{12}A_{21} \end{cases} \tag{58}$$

This means that, since the sum between the real part of eigenvalues is always negative (being the damping coefficient of the NES positive), if the product between them is positive, both of them have to be negative, so the equilibrium point is stable, while if the product is negative, the real part of one eigenvalue is necessarily positive, so the equilibrium point is unstable. It is concluded that the unstable zones of the SIM are those for which $A_{11}A_{22} - A_{12}A_{21} < 0$.

3.3. Slow time scale

Here the goal is to study the evolution of the SIM at the slow time scale τ_1 and to study the system at slow time scale around the SIM (Starosvetsky and Gendelman, 2008), to investigate its behavior near resonance. In order to do that, equilibrium and singular points have to be found starting from the first equilibrium equation at order ε^1, Eq. (50), written as:

$$\frac{\partial\beta_1}{\partial\tau_1} = \mathbb{E}_1(\beta_1, \beta_2, \beta_1^*, \beta_2^*) \tag{59}$$

where:

$$\mathbb{E}_1(\beta_1, \beta_2, \beta_1^*, \beta_2^*) = \frac{\sigma}{2i}\beta_1 - \frac{\hat{C}_j}{2D}\beta_1 - \frac{1}{2i}(\beta_2 - \sigma\beta_1)$$

$$- \frac{3}{8i}\tilde{k}_N\left(\chi_j - 1\right)\beta_2^2\beta_2^* - \frac{1}{2}\tilde{c}_N\left(\chi_j - 1\right)\beta_2 + \frac{\Omega}{2\pi}\int_0^{\frac{2\pi}{\Omega}} \Gamma e^{-i\Omega\tau}d\tau \tag{60}$$

Moreover, the evolution of the SIM $\mathbb{S}$ at the current time scale τ_1 has to be considered as:

$$\begin{cases} \frac{\partial\mathbb{S}}{\partial\tau_1} = \frac{\partial\mathbb{S}}{\partial\beta_1}\frac{\partial\beta_1}{\partial\tau_1} + \frac{\partial\mathbb{S}}{\partial\beta_2}\frac{\partial\beta_2}{\partial\tau_1} + \frac{\partial\mathbb{S}}{\partial\beta_1^*}\frac{\partial\beta_1^*}{\partial\tau_1} + \frac{\partial\mathbb{S}}{\partial\beta_2^*}\frac{\partial\beta_2^*}{\partial\tau_1} = 0 \\ \frac{\partial\mathbb{S}^*}{\partial\tau_1} = \frac{\partial\mathbb{S}^*}{\partial\beta_1}\frac{\partial\beta_1}{\partial\tau_1} + \frac{\partial\mathbb{S}^*}{\partial\beta_2}\frac{\partial\beta_2}{\partial\tau_1} + \frac{\partial\mathbb{S}^*}{\partial\beta_1^*}\frac{\partial\beta_1^*}{\partial\tau_1} + \frac{\partial\mathbb{S}^*}{\partial\beta_2^*}\frac{\partial\beta_2^*}{\partial\tau_1} = 0 \end{cases} \tag{61}$$

This system of equations can be reorganized in matrix form as:

$$\underbrace{\begin{bmatrix} \frac{\partial\mathbb{S}}{\partial\beta_2} & \frac{\partial\mathbb{S}}{\partial\beta_2^*} \\ \frac{\partial\mathbb{S}^*}{\partial\beta_2} & \frac{\partial\mathbb{S}^*}{\partial\beta_2^*} \end{bmatrix}}_{\mathbf{J_2}}\begin{pmatrix} \frac{\partial\beta_2}{\partial\tau_1} \\ \frac{\partial\beta_2^*}{\partial\tau_1} \end{pmatrix} = -\begin{bmatrix} \frac{\partial\mathbb{S}}{\partial\beta_1} & \frac{\partial\mathbb{S}}{\partial\beta_1^*} \\ \frac{\partial\mathbb{S}^*}{\partial\beta_1} & \frac{\partial\mathbb{S}^*}{\partial\beta_1^*} \end{bmatrix}\begin{pmatrix} \frac{\partial\beta_1}{\partial\tau_1} \\ \frac{\partial\beta_1^*}{\partial\tau_1} \end{pmatrix} \tag{62}$$

By calling $\mathbf{J_2}$ the Jacobian matrix of the SIM with respect to (β_2, β_2^*) the following systems can be written, for equilibrium and singular points respectively:

$$\begin{cases} \mathbb{E}_1 = 0 \\ \mathbb{S} = 0 \\ \det(\mathbf{J_2}) \neq 0 \end{cases} \qquad \begin{cases} \mathbb{E}_1 = 0 \\ \mathbb{S} = 0 \\ \det(\mathbf{J_2}) = 0 \end{cases} \tag{63}$$

Computing matrix $\mathbf{J_2}$, it turns out that $\mathbf{J_2} = -\mathbf{A}$, which involves that singular points of the system are located in correspondence of the stability borders.

Equilibrium points are found investigating the first two equations of the first system in Eq. (63), namely Eqs. (60) and (52), to get an equation containing N_2, having as unknown the detuning parameter σ, such that a simple second order algebraic equation has to be solved for different values of N_2. Setting $F = 3/4\tilde{k}_N\beta_2\beta_2^*$ and $\hat{\gamma} = \Omega/(2\pi)\int_0^{2\pi/\Omega}\Gamma e^{-i\Omega\tau}d\tau$, the first two equations of the system give:

$$c_1\sigma^2 + c_2\sigma + c_3 = 0 \tag{64}$$

where:

$$c_1 = N_2^2\left[\left(\frac{1}{\chi_j} - \frac{F}{\chi_j}\right)^2 + \frac{\tilde{c}_N^2}{\chi_j^2}\right] \tag{65}$$

$$c_2 = N_2^2\left(\frac{F^2(\chi_j - 1)}{\chi_j} - \frac{F(\chi_j - 1)}{\chi_j} + \frac{F}{\chi_j} - \frac{1}{\chi_j} + \frac{\tilde{c}_N^2(\chi_j - 1)}{\chi_j}\right) \tag{66}$$

$$c_3 = N_2^2\left(\frac{F^2(\chi_j - 1)^2}{4} + \frac{F(\chi_j - 1)}{2} + \frac{\tilde{c}_N^2(\chi_j - 1)^2}{4} + \frac{1}{4}\right.$$
$$\left. + \frac{\hat{C}_j^2F^2}{4\chi_j^2} - \frac{\hat{C}_j^2F}{2\chi_j^2} + \frac{\hat{C}_j\tilde{c}_N}{2} + \frac{\hat{C}_j^2}{4\chi_j^2} + \frac{\hat{C}_j^2\tilde{c}_N^2}{4\chi_j^2}\right) - \left|\frac{-\hat{\gamma}}{i}\right|^2 \tag{67}$$

Resolution of Eq. (64) gives maximum two values of σ for every assigned N_2, where only real values of σ have a physical meaning. Moreover, the relationship between N_1 and σ can be obtained through Eq. (52), thus getting the frequency response curves, i.e. the relationships between the amplitudes of response N_1 and N_2 and the frequency, here represented by the detuning parameter σ. From these curves, different types of responses can be obtained as function of σ:

(i) Periodic Response: for stable equilibrium points, with the system oscillating in time with a certain period, asymptotically tending to equilibrium.
(ii) Modulated Response: generally speaking this response can be detected if the system presents fold singularities, i.e. when equilibrium points (obtained from $\mathbb{E}_1 = 0$ around the SIM) and singular points (for which $\det(\mathbf{J_2}) = 0$) coincide (see Eq. (63)) (Gendelman and Starosvetsky, 2006; Starosvetsky and Gendelman, 2008;

Lamarque et al., 2011). Moreover, if the equilibrium point is positioned in the unstable zone of the SIM, the system will also present the modulated response, corresponding to repeated jumps between the limit points of the SIM (Hurel et al., 2019a). Physically speaking, this response is similar to beating.

(iii) Isola: the system can present isolas as well. This isolated branch of the frequency response curve can appear for some ranges of amplitude of the external excitation and out of them it reintegrates to the main branch. It can be seen that the frequency response curve in the $N_1 - N_2$ plane can be superimposed to the SIM (Fig. 14(b)). In general, isolas have higher energy levels causing amplification in the response. More details can be found in da Silveira Zanin et al. (2022).

It should be mentioned that the backbone curve (Nayfeh and Mook, 1995) of the system can be obtained too from Eq. (64), via setting damping and amplitudes of forcing to zero; for nonlinear conservative systems, this curve provides the amplitude dependency of the frequency.

4. Types of load

To show the capability of the NES to reduce vibrations related to various types of loads, with different frequency contents, some cases are here presented. Loads are resumed in Table 1 and shown in Fig. 5 and results reported in Section 5.

4.1. Uniform load

A vertical, sinusoidal, uniformly distributed load with frequency Ω_F is applied on the upper flange of the beam (p is in N/m^2). The introduction of non-dimensional time has led to the non-dimensional term Ω, written in Eq. (47). It can be useful to write $\Gamma = \gamma \sin(\Omega\tau)$ where γ can be derived from Table 1, so that $\hat{\gamma}$ appearing in Eq. (67) is equal to $\gamma/(2i)$. This case is identified as UL-1.

Moreover, a similar case is considered, but with the load applied only in the mid upper flange of the cross section of the beam, i.e. between the points of intersection of inclined webs with the upper flange, identified as UL-2.

4.2. Punctual load

A vertical, sinusoidal, punctual load with frequency Ω_F is applied at half-length of the beam (p is in N/m, as it has to be written as the ratio between the punctual load in N and the dimension of the element of the cross-section along s). Also in this case $\hat{\gamma}$ is equal to $\gamma/(2i)$. This case is identified as PL.

4.3. Train of moving loads

A train of moving loads, representing a series of N_v vehicles moving on the bridge at constant speed v_V and distance d, is applied on the upper flange of the beam. The frequency of every load is $\Omega_F = n_j \pi v_V / L$ (Yang et al., 2004). Expressions in Table 1 are meant for each vehicle, where $t_j = (j-1)d/v_V$ is the arriving time of the jth load on the beam and $t_j + L/v_V$ is the time when the vehicle leaves the beam. Only the numerical solution of Eqs. (39), (40) has been explored using a Runge–Kutta method since, due to the characteristics of the beam, an extremely high speed should be taken to consider a 1:1 resonance, thus resulting in an unrealistic scenario. This case is identified as ML.

4.4. Seismic load

For seismic action, if the NES is disregarded, both analytical and numerical solutions can be obtained, while, for the beam with NES, only the numerical solution of Eqs. (39), (40) through a Runge–Kutta method is considered, since it is not possible to apply the aforementioned procedure with a 1:1 resonance, as the earthquake has a wide spectrum of frequencies. Moreover, in general, in Eqs. (27)–(28) the hypothesis that only the jth vibration mode contributes to the beam response is no more valid and a sufficient number of vibration modes should be considered, and the presence of nonlinear stiffness and damping terms of the NES couples all these vibration modes. However, for the case under study, for the beam without NES it has been seen that, due to the characteristics of the beam itself and of the chosen earthquake, the difference between the analytical solution keeping only the 1st vibration mode, and that with more than one mode is negligible, meaning that for this specific case it is possible to proceed with only one mode.

The earthquake is considered as a vertical ground motion $v_g(t)$, applied to both supports of the beam, so that displacements $v(s,z,t)$ and $y_N(t)$ are relative to the base. As a consequence, the ground acceleration is $\ddot{v}_g(t)$ and, considering the mass per unit area m seen in Eq. (9), the load terms are reported in Table 1. This case is identified as SL.

5. Results

Geometrical and mechanical properties of the beam are presented in Fig. 6 and in Table 2, while those of the NES are written in Table 3. It should be specified that the choice of the NES parameters does not come from a rigorous optimization procedure (Boroson et al., 2017), so it is plausible that even better results can be found by changing NES properties in terms of efficiency (see for example Lamarque et al., 2011 where different trends of the SIM are identified as the parameters vary.)

In Fig. 7 the analytical SIM, found using Eq. (54), with stability borders (in red), determined in accordance to Eq. (58), is shown together with a numerical solution given by the resolution of Eqs. (39)–(40) without external load, subjected to some non-trivial initial conditions marked as "x". The unstable zone is represented by a dashed line and it can be noted that, for these initial conditions, the solution oscillates in time around the second branch and then in correspondence of the stability border jumps on the first branch to go to zero, being the unstable zone physically unattainable.

The backbone curve is shown in Fig. 8 together with some frequency response curves for different load amplitudes in the case UL-1. As it can be seen, it is the locus of the peak amplitudes and it shows that by increasing the amplitude of the external load, the NES performance increases and different kinds of equilibrium points can be obtained.

5.1. Uniform load

5.1.1. Case 1

A UL-1 case with amplitude $p = 6.0 \times 10^1$ N/m^2 and frequency equal to that of the first vibration mode (indicated as Φ_1 in Fig. 3) $\Omega_F = \omega_1 = 15.05$ rad/s is considered.

From Fig. 9(a) it can be noticed that for this type of load the NES is well activated and, in Figs. 9(b), 9(c), it is shown that in function of the value of the detuning parameter, it is possible to have 1, 2 or even 3 solutions of different nature, depending on initial conditions. Moreover, in Fig. 9(b) a comparison between frequency response curves of the beam with and without NES highlights a general reduction of displacement on the beam when the nonlinear device is engaged.

Fig. 10(a) shows that for $\sigma = 0.65$ the equilibrium point (represented by the circle) moves in time around the SIM and, when it attains the stability border, it bifurcates, jumping on the other branch. The same behavior, describing a modulated response, can be found in Figs. 10(b), 10(c) where bifurcations in time are evident; furthermore in the same

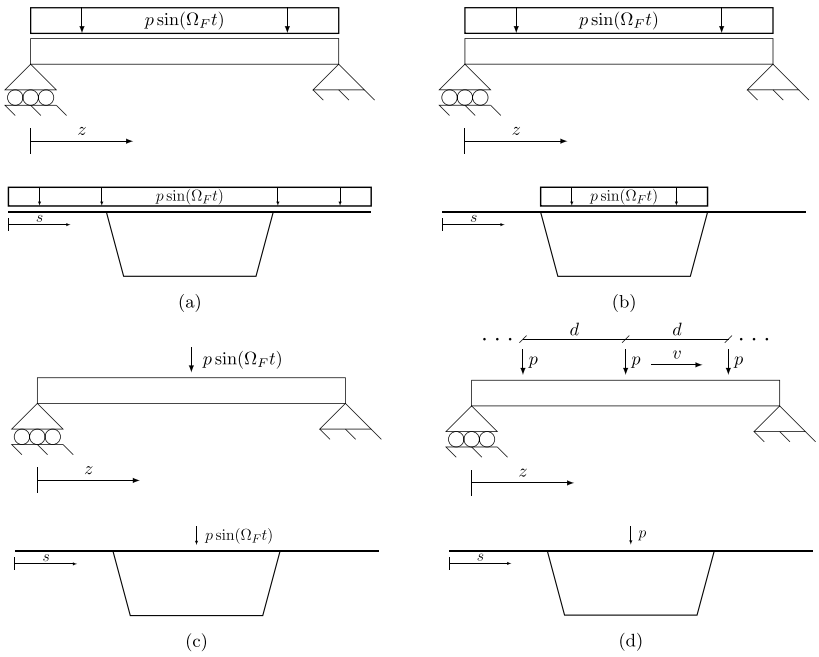

Fig. 5. Schematic representation of different types of loads in longitudinal and transversal planes: (a) UL-1, (b) UL-2, (c) PL, (d) ML. Refer to Section 4 for definitions of abbreviations.

Table 1
Characteristics of different types of loads.

Type of load	$f_y(s,z,t)$	$\mathbf{p}^0_\Omega$	$\epsilon\Gamma$ for $n_j = 1,5,\ldots$
Uniform	$p\sin(\Omega_F t)$	$\int_S p\mathbf{V}(s)ds$	$\frac{4}{n_j\pi\omega_j^2 b_1}\frac{\mathbf{\Theta}_j^T\mathbf{p}^0_\Omega}{\mathbf{\Theta}_j^T\mathbf{M}_j\mathbf{\Theta}_j}\sin(\Omega\tau)$
Punctual	$p\sin(\Omega_F t)\delta(z-L/2)$	$\int_S p\mathbf{V}(s)ds$	$\frac{2}{b_1 L\omega_j^2}\frac{\mathbf{\Theta}_j^T\mathbf{p}^0_\Omega}{\mathbf{\Theta}_j^T\mathbf{M}_j\mathbf{\Theta}_j}\sin(\Omega\tau)$
Moving	$p\delta(z-v_V(t-t_j))$	$\int_S p\mathbf{V}(s)ds$	$\frac{2}{b_1 L\omega_j^2}\frac{\mathbf{\Theta}_j^T\mathbf{p}^0_\Omega}{\mathbf{\Theta}_j^T\mathbf{M}_j\mathbf{\Theta}_j}\sin(\Omega(\tau-\tau_j))$
Seismic	$m\ddot{v}_g(t)$	$\int_S m\big(\mathbf{U}(s)\sin(\alpha)+\mathbf{V}(s)\cos(\alpha)\big)ds$	$\frac{4}{n_j\pi\omega_j^2 b_1}\frac{\mathbf{\Theta}_j^T\mathbf{p}^0_\Omega}{\mathbf{\Theta}_j^T\mathbf{M}_j\mathbf{\Theta}_j}\ddot{v}_g(t)$

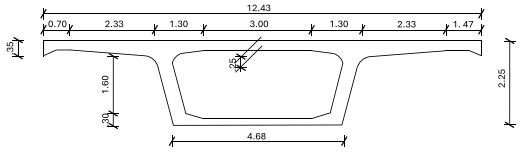

Fig. 6. Beam cross-section (measures in m).

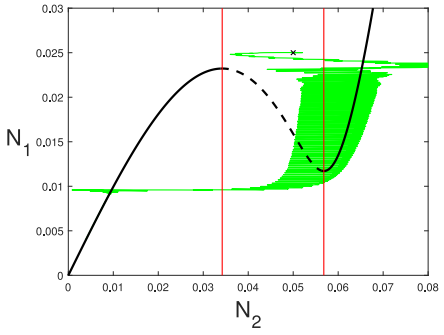

Fig. 7. Analytical and numerical SIM. (For interpretation of the references to color in this figure legend, the reader is referred to the web version of this article.)

Table 2
Geometrical and mechanical properties of the beam.

m_{tot} (t)	L (m)	b_1 (m)	ξ_j	E (N/m^2)
571	40.5	3.15	0.1%	3.108×10^{10}

Table 3
Parameters of the NES.

m_N (kg)	c_N (N s/m)	k_N (N/m^3)	z_N (m)
650	2×10^3	6×10^6	$L/2$

figures N_1 and N_2 are plotted as envelopes of r and a respectively, having the meaning of energies.

In Fig. 11(a) the displacement of the beam and of the NES is shown, normalized with respect to the beam length, while in Fig. 11(b) the response of the beam with and without NES highlights the reduction of its displacement as well as the modulated response.

5.1.2. Case 2

A UL-1 case with amplitude $p = 6.0\times10^1$ N/m^2 and frequency equal to that of the first vibration mode (flexural mode) $\Omega_F = \omega_1 = 15.05$ rad/s with $\sigma = 0$ is considered.

In this case the response is periodic, with the equilibrium point oscillating in time and attaining to an asymptotic value, as shown in

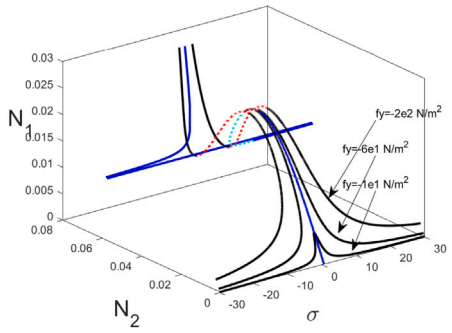

Fig. 8. Frequency response curves of the system and backbone curve (in blue and cyan). (For interpretation of the references to color in this figure legend, the reader is referred to the web version of this article.)

Figs. 12(a), 12(b); the values of N_1 and N_2 found solving the numerical problem are almost the same as the analytical ones identified by the vertical line at $\sigma = 0$ in Figs. 9(b), 9(c), highlighting once again the validity of the analytical model. Moreover, in Fig. 13(a), it can be seen that the displacement of the NES is high enough to reduce the displacement of the beam as shown in Fig. 13(b). It should be noticed that, even if the behavior of the NES is not optimal, displacements are compatible with those expected on a real beam.

5.1.3. Case 3

A UL-2 case with amplitude $p = 2.0 \times 10^4$ N/m^2 and frequency equal to that of the fifth vibration mode (indicated as $\mathbf{\Phi}_5$ in Fig. 3) $\Omega_F = \omega_5 = 87.21$ rad/s is considered.

Results reported in Figs. 14(a), 14(b), 14(c) are quite interesting, since they show the onset on an isola (see for example Guo et al., 2022; Kuether et al., 2015), which can be dangerous for the beam due to the higher energy level (note that stable and unstable zones are referred to those of the SIM). Figs. 15(a), 15(b) show once again the excellent correspondence of the numerical solution and the analytical one, as can be seen by looking at the values intercepted by the vertical lines in Fig. 14(c). Moreover, in Figs. 16(a), 16(b) the reduction of the displacement on the beam, due to the Modulated Response of the NES is still evident, meaning that the same NES can be used to control a different type of load with different frequency, which has been detected thanks to GBT: in fact, it should be underlined that in this case GBT is fundamental to detect this vibration mode, which, as can be seen in Fig. 3, exhibits the deformation of the cross-section in its own plane.

5.2. Punctual load

A PL case with amplitude $p = 3.0 \times 10^4$ N (divided by the dimension of the cross-section element along s to have a load for unit length) and frequency equal to that of the first vibration mode is considered.

Results are qualitatively the same of those shown for uniform load, as can be seen in Fig. 17(a) where the isola is also present, and in Fig. 17(b), showing the ability of the NES to reduce vibrations on this type of beam also for this type of load.

5.3. Train of moving loads

Different combinations of parameters can be considered for this type of load. In this case $N_v = 80$ vehicles, at a distance $d = 20$ m with a speed $v_V = 70$ m/s and with amplitude $p = 3.0 \times 10^5$ N is considered.

Results reported in Figs. 18(a), 18(b) show a reduction of the vertical displacement of the beam with NES, both during the transit of vehicles on the bridge and in free oscillations. Even though the NES is activated, the reduction is not so impressive in this case, and it can be better appreciated in the tail of the Figures, when all the vehicles have passed through the beam; it is likely that the high number of parameters involved for the load, in addition to those of the NES, do not permit an ideal reduction in vibrations. In Tables 4–5 some results are reported, showing the influence of different vehicle parameters on vibration control; values are $(v_N^{w/} - v_N^{w/o})/v_N^{w/o}$ in percentage. In particular, from Table 4 it can be noticed that if vehicles are too close or too far, with respect to the beam length, the NES could increase the displacement (positive difference) rather than reducing it, above all for higher speed values. On the other hand, Table 5 shows that for some combinations of N_v and v_V the reduction is more effective. Furthermore, it should be stated that the chosen speed of vehicles is quite far from the critical one, which for the characteristics of this beam is too high to have a physical meaning, so the reduction may not be optimal.

Table 4
Influence of d and v_V on vibrations reduction with $p = 3.0 \times 10^5$ N/m^2 and $N_v = 80$. Values represent $(v_N^{w/} - v_N^{w/o})/v_N^{w/o}$ in percentage.

v_V \ d	15 (m)	20 (m)	30 (m)
36 (m/s)	−4.56	−29.41	−0.23
50 (m/s)	−6.25	−15.88	+30.12
70 (m/s)	+44.75	−38.85	+22.92

Table 5
Influence of N_v and v_V on vibrations reduction with $p = 3.0 \times 10^5$ N/m^2 and $d = 20$ m. Values represent $(v_N^{w/} - v_N^{w/o})/v_N^{w/o}$ in percentage.

v_V \ N_v	10	20	50
36 (m/s)	−2.71	−6.90	−24.79
50 (m/s)	−2.06	+7.34	−28.49
70 (m/s)	−9.25	−13.43	+1.29

5.4. Seismic load

A SL case has been considered with ground acceleration $\ddot{v}_g(t)$ taken as the time history of a past earthquake (L'Aquila, Italy, 2009), chosen such that the range of frequencies of the event, identified by its spectrum, was around the 1st frequency of the beam, with a vertical Peak Ground Acceleration - PGA, slightly increased, of 0.52 g (Fig. 19(a)). Numerical results shown in Figs. 19(b), 19(c), highlight the instant when the NES is activated, almost corresponding to the moment when the seismic acceleration reaches its peak value, and show an evident reduction of displacement of the beam with the NES, even if the maximum displacement is not reduced. This application demonstrates the validity of the NES in reducing vibrations related to real loading scenarios, which can otherwise cause severe problems on bridge decks.

6. Conclusions

A full-scale beam has been studied with the goal of reducing vibrations caused by different types of loads with different frequencies. Due to its shape, the beam has been modeled through Generalized Beam Theory to take into account aspects like the deformation of the cross-section in its own plane and to consider vibration modes (like torsional, local or mixed ones) which cannot be considered with simpler beam theories. The beam, linked to a Nonlinear Energy Sink, has been studied through the Complexification Averaging Method, highlighting a good reduction in beam vibrations for 1:1 resonant loads, with different behaviors (periodic, modulated response, isolas). A lower reduction for non-resonant loads has been shown, like earthquake or train of moving loads.

Possible future developments include an optimization analysis to find the best parameters for the Nonlinear Energy Sink, the use of

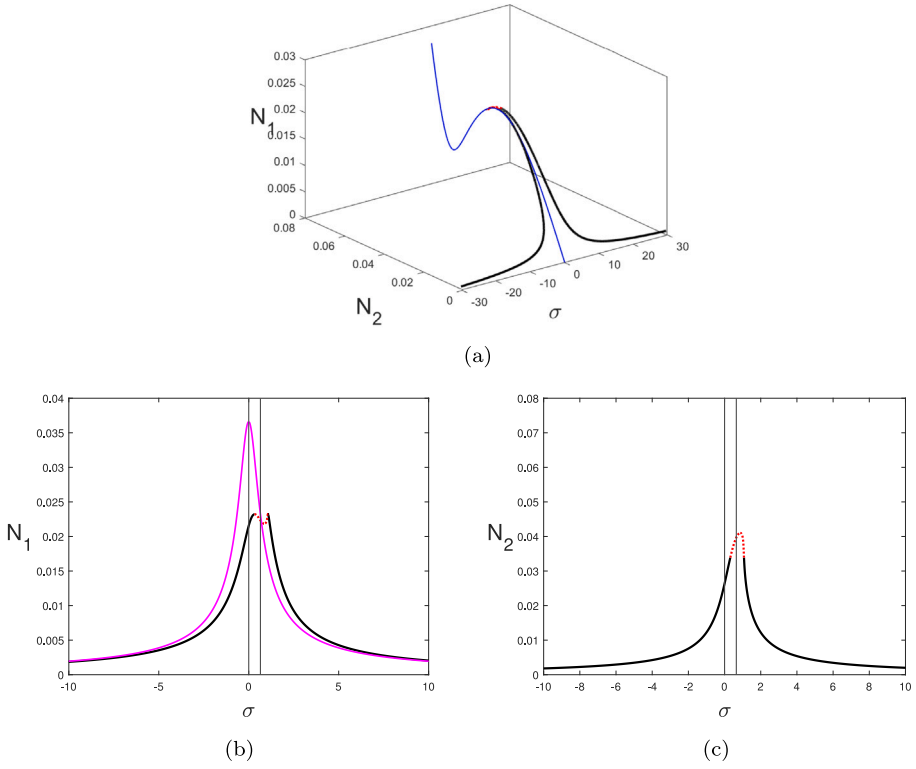

Fig. 9. Different views of the frequency response curve for the system under UL-1 load for $p = 6.0 \times 10^1$ N/m^2: (a) Three dimensional view in $N_1 - N_2 - \sigma$ (the unstable zone of the SIM is showed in dashed red) with SIM (in blue); (b) Two dimensional view in $N_1 - \sigma$ with the frequency response curve of the beam without NES (in magenta); (c) Two dimensional view in $N_2 - \sigma$. Vertical lines represent values of σ investigated in next Figures. (For interpretation of the references to color in this figure legend, the reader is referred to the web version of this article.)

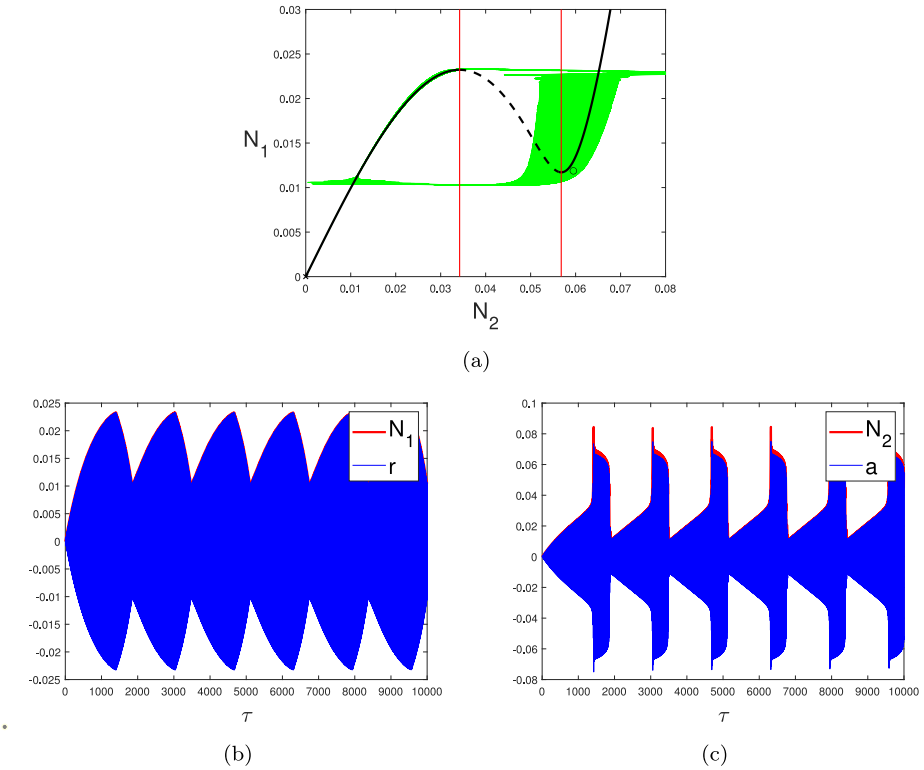

Fig. 10. SIM and numerical results for the system under UL-1 load for $p = 6.0 \times 10^1$ N/m^2, $\sigma = 0.65$: (a) $N_1 - N_2$ with SIM; (b) Time history of N_1 and r; (c) Time history of N_2 and a. Numerical results are obtained from direct numerical integration of Eqs. (39)–(40) with zero initial conditions.

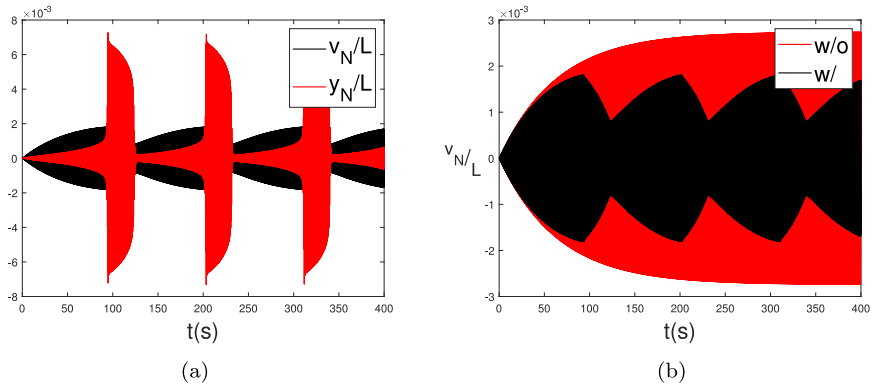

Fig. 11. Numerical results for the system under UL-1 load for $p = 6.0 \times 10^1$ N/m^2, $\sigma = 0.65$: (a) Time histories of v_N/L and y_N/L; (b) Time histories of v_N/L with and without NES. Numerical results are obtained from direct numerical integration of Eqs. (39)–(40) with zero initial conditions.

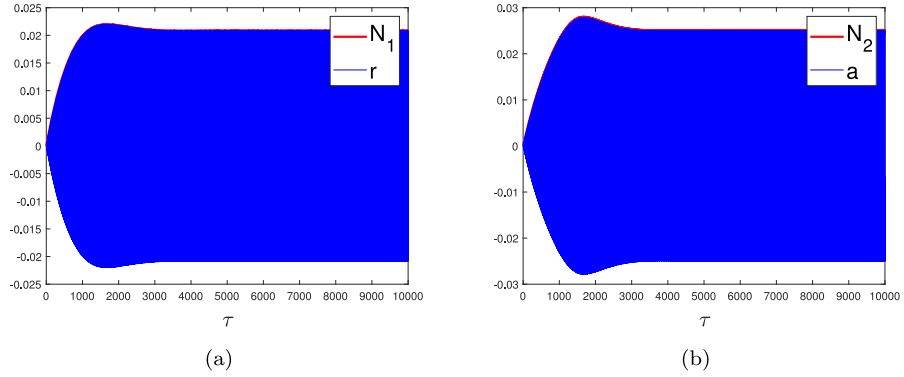

Fig. 12. Numerical results for the system under UL-1 load for $p = 6.0 \times 10^1$ N/m^2, $\sigma = 0$: (a) Time history of N_1 and r; (b) Time history of N_2 and a. Numerical results are obtained from direct numerical integration of Eqs. (39)–(40) with zero initial conditions.

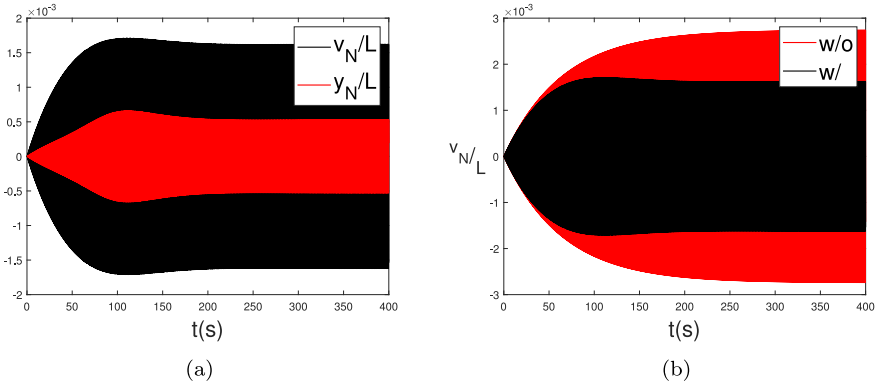

Fig. 13. Numerical results for the system under UL-1 load for $p = 6.0 \times 10^1$ N/m^2, $\sigma = 0$: (a) Time histories of v_N/L and y_N/L; (b) Time histories of v_N/L with and without NES. Numerical results are obtained from direct numerical integration of Eqs. (39)–(40) with zero initial conditions.

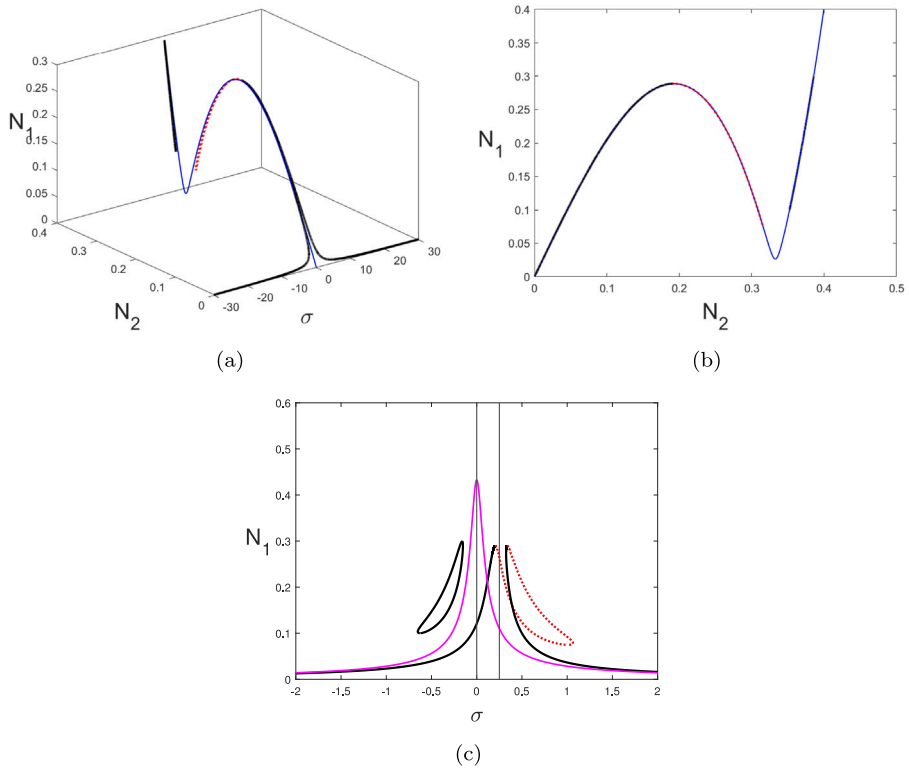

Fig. 14. Different views of the frequency response curve for the system under UL-2 load for $p = 2.0 \times 10^4$ N/m^2: (a) Three dimensional view in $N_1 - N_2 - \sigma$ (the unstable zone of the SIM is showed in dashed red) with SIM (in blue); (b) Two dimensional view in $N_1 - N_2$ with SIM; (c) Two dimensional view in $N_1 - \sigma$ with the frequency response curve of the beam without NES (in magenta). Vertical lines represent values of σ investigated in next Figures. (For interpretation of the references to color in this figure legend, the reader is referred to the web version of this article.)

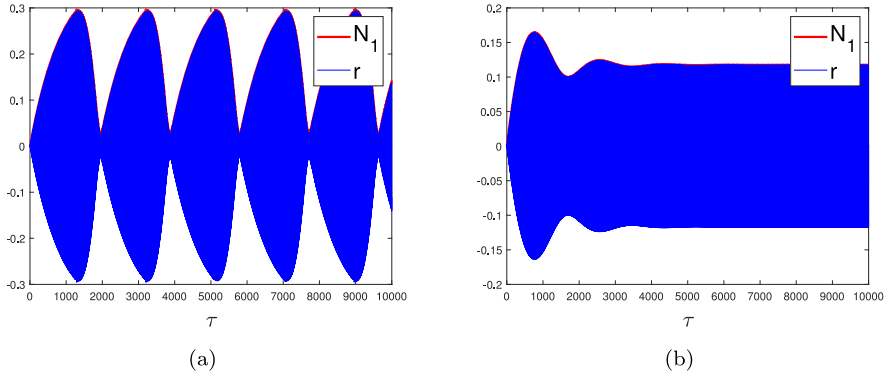

Fig. 15. Numerical results for the system under UL-2 load for $p = 2.0 \times 10^4$ N/m^2: (a) Time history of N_1 and r for $\sigma = 0.25$; (c) Time history of N_1 and r for $\sigma = 0$. Numerical results are obtained from direct numerical integration of Eqs. (39)–(40) with zero initial conditions.

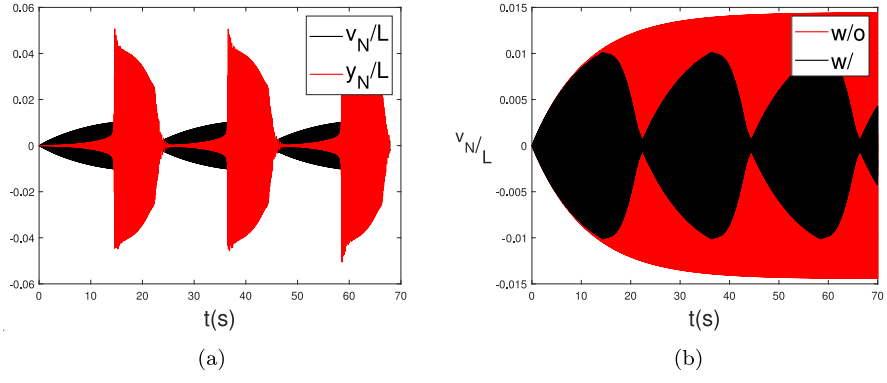

Fig. 16. Numerical results for the system under UL-2 load for $p = 2.0 \times 10^4$ N/m^2, $\sigma = 0.25$: (a) Time histories of v_N/L and y_N/L; (b) Time histories of v_N/L with and without NES. Numerical results are obtained from direct numerical integration of Eqs. (39)–(40) with zero initial conditions.

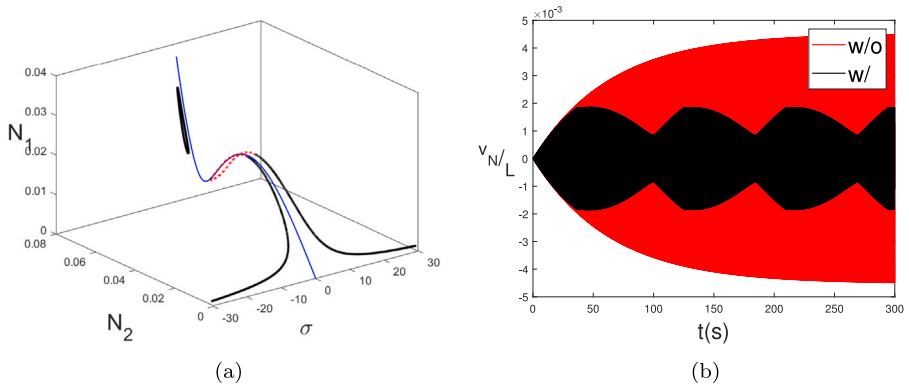

Fig. 17. (a) Three dimensional view of the frequency response curve for the system under PL load for $p = 3.0 \times 10^4$ N (the unstable zone of the SIM is showed in dashed red) with SIM (in blue); (b) Time histories of v_N/L with and without NES for $\sigma = 0.5$. Numerical results are obtained from direct numerical integration of Eqs. (39)–(40) with zero initial conditions. (For interpretation of the references to color in this figure legend, the reader is referred to the web version of this article.)

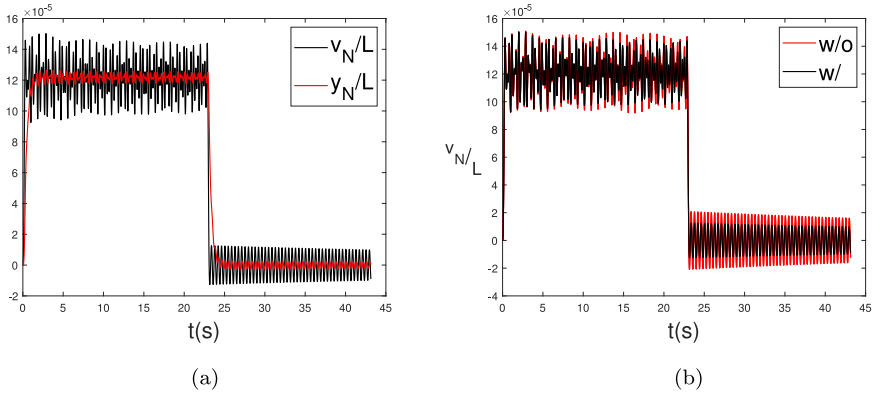

Fig. 18. Numerical results for the system under ML load for $p = 3.0 \times 10^5$ N/m^2, $N_v = 80$, $d = 20$ m, $v_V = 70$ m/s: (a) Time histories of v_N/L and y_N/L; (b) Time histories of v_N/L with and without NES. Numerical results are obtained from direct numerical integration of Eqs. (39)–(40) with zero initial conditions.

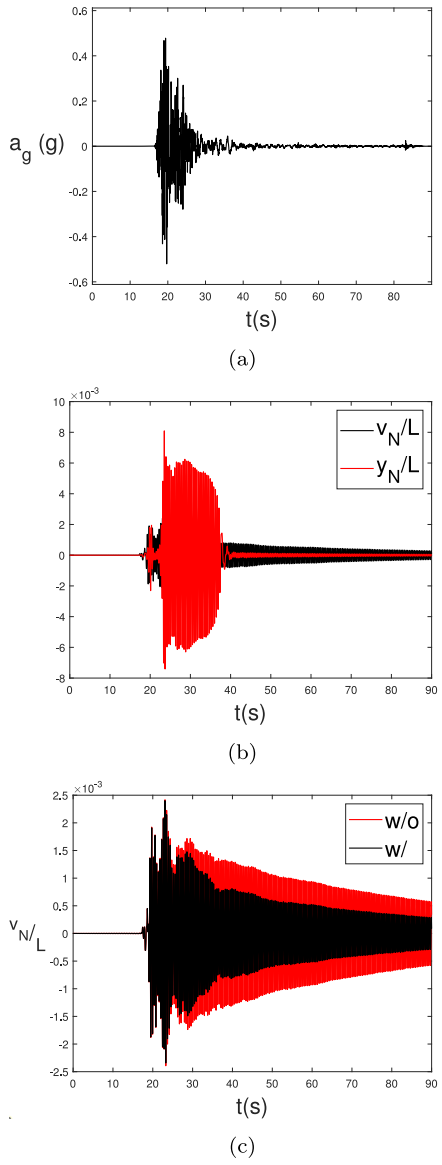

Fig. 19. Numerical results for the system under SL load: (a) Time history of the event; (b) Time histories of v_N/L and y_N/L; (c) Time histories of v_N/L with and without NES. Numerical results are obtained from direct numerical integration of Eqs. (39)–(40) with zero initial conditions.

different types of nonlinearities (e.g. non-smooth ones) for the device and the implementation of geometrical and mechanical nonlinearities in the beam model.

CRediT authorship contribution statement

Andrea De Flaviis: Writing – review & editing, Writing – original draft, Visualization, Validation, Software, Resources, Methodology, Investigation, Formal analysis, Data curation, Conceptualization. **Alireza Ture Savadkoohi:** Writing – review & editing, Validation, Supervision, Resources, Project administration, Methodology, Investigation, Conceptualization. **Daniele Zulli:** Writing – review & editing, Validation, Supervision, Resources, Project administration, Methodology, Investigation, Funding acquisition, Conceptualization.

Funding sources

The first author has received research support from Company "Dimensione Solare S.r.l." as part of the financial program of his PhD thesis.

Declaration of competing interest

The authors declare that they have no known competing financial interests or personal relationships that could have appeared to influence the work reported in this paper.

Data availability

Data will be made available on request.

References

Bakre, S.V., Jangid, R.S., 2007. Optimum parameters of tuned mass damper for damped main system. Struct. Control Health Monit. 14 (3), 448–470. http://dx.doi.org/10.1002/stc.166.

Bebiano, R., Camotim, D., Silvestre, N., 2013. Dynamic analysis of thin-walled members using Generalised Beam Theory (GBT). Thin-Walled Struct. 72, 188–205. http://dx.doi.org/10.1016/j.tws.2013.07.004.

Bebiano, R., Gonçalves, R., Camotim, D., 2015. A cross-section analysis procedure to rationalise and automate the performance of GBT-based structural analyses. Thin-Walled Struct. 92, 29–47. http://dx.doi.org/10.1016/j.tws.2015.02.017.

Boroson, E., Missoum, S., Mattei, P.-O., Vergez, C., 2017. Optimization under uncertainty of parallel nonlinear energy sinks. J. Sound Vib. 394, 451–464. http://dx.doi.org/10.1016/j.jsv.2016.12.043.

Camotim, D., Silvestre, N., Basaglia, C., Bebiano, R., 2008. GBT-based buckling analysis of thin-walled members with non-standard support conditions. Thin-Walled Struct. 46 (7–9), 800–815. http://dx.doi.org/10.1016/j.tws.2008.01.019.

Carr, J., 1981. Applications of Centre Manifold Theory. Vol. 35, Applied Mathematical Sciences. Springer-Verlag, New York - Heidelberg - Berlin, http://dx.doi.org/10.1007/978-1-4612-5929-9.

Casalotti, A., Arena, A., Lacarbonara, W., 2014. Mitigation of post-flutter oscillations in suspension bridges by hysteretic tuned mass dampers. Eng. Struct. 69, 62–71. http://dx.doi.org/10.1016/j.engstruct.2014.03.001.

Chen, Y., Qian, Z., Chen, K., Tan, P., Tesfamariam, S., 2019. Seismic performance of a nonlinear energy sink with negative stiffness and sliding friction. Struct. Control Health Monit. 26 (11), e2437. http://dx.doi.org/10.1002/stc.2437.

da Silveira Zanin, C., Ture Savadkoohi, A., Baguet, S., Dufour, R., Hurel, G., 2022. Nonlinear vibratory energy exchanges in a meta-cell. Int. J. Non-Linear Mech. 146, 104148. http://dx.doi.org/10.1016/j.ijnonlinmec.2022.104148.

Davies, J., Leach, P., 1992. Some Applications of Generalized Beam Theory. International Specialty Conference on Cold-Formed Steel Structures. 2.

Davies, J., Leach, P., 1994. First-order Generalised Beam Theory. J. Constr. Steel Res. 31 (2), 187–220. http://dx.doi.org/10.1016/0143-974X(94)90010-8.

De Flaviis, A., Alaggio, R., Zulli, D., 2024. Generalized Beam Theory for the static and dynamic response of a bridge deck with Structural Health Monitoring purposes. Procedia Struct. Integr. 62, 871–878. http://dx.doi.org/10.1016/j.prostr.2024.09.117.

Den Hartog, J.P., 1947. Mechanical Vibrations. McGraw-Hill Book Company, New York and London.

Ding, H., Chen, L.-Q., 2020. Designs, analysis, and applications of nonlinear energy sinks. Nonlinear Dynam. 100, 3061–3107. http://dx.doi.org/10.1007/s11071-020-05724-1.

Frahm, H., 1911. Device for damping vibrations of bodies. US Patent 989, 958.

Fujino, Y., Abé, M., 1993. Design formulas for tuned mass dampers based on A perturbation technique. Earthq. Eng. Struct. Dyn. 22 (10), 833–854. http://dx.doi.org/10.1002/eqe.4290221002.

Gattulli, V., Di Fabio, F., Luongo, A., 2001. Simple and double Hopf bifurcations in aeroelastic oscillators with tuned mass dampers. J. Franklin Inst. 338 (2), 187–201. http://dx.doi.org/10.1016/S0016-0032(00)00077-6.

Gendelman, O., Manevitch, L.I., Vakakis, A.F., M'Closkey, R., 2000. Energy Pumping in Nonlinear Mechanical Oscillators: Part I—Dynamics of the Underlying Hamiltonian systems. J. Appl. Mech. 68 (1), 34–41. http://dx.doi.org/10.1115/1.1345524.

Gendelman, O.V., Starosvetsky, Y., 2006. Quasi-Periodic Response Regimes of Linear Oscillator Coupled to Nonlinear Energy Sink Under Periodic Forcing. J. Appl. Mech. 74 (2), 325–331. http://dx.doi.org/10.1115/1.2198546.

Gendelman, O., Starosvetsky, Y., Feldman, M., 2008. Attractors of harmonically forced linear oscillator with attached nonlinear energy sink I: Description of response regimes. Nonlinear Dynam. 51, 31–46. http://dx.doi.org/10.1007/s11071-006-9167-0.

Georgiades, F., Vakakis, A., 2007. Dynamics of a linear beam with an attached local nonlinear energy sink. Commun. Nonlinear Sci. Numer. Simul. 12 (5), 643–651. http://dx.doi.org/10.1016/j.cnsns.2005.07.003.

Gonçalves, R., Camotim, D., Basaglia, C., Martins, A., Peres, N., 2023. Latest developments on the analysis of thin-walled structures using Generalised Beam Theory (GBT). J. Constr. Steel Res. 204, 107858. http://dx.doi.org/10.1016/j.jcsr.2023.107858.

Gourdon, E., Lamarque, C.-H., 2005. Energy Pumping with Various Nonlinear Structures: Numerical Evidences. Nonlinear Dynam. 40, 281–307. http://dx.doi.org/10.1007/s11071-005-6610-6.

Guo, H., Yang, T., Chen, Y., Chen, L.-Q., 2022. Singularity analysis on vibration reduction of a nonlinear energy sink system. Mech. Syst. Signal Process. 173, 109074. http://dx.doi.org/10.1016/j.ymssp.2022.109074.

Hurel, G., Ture Savadkoohi, A., Lamarque, C.-H., 2019a. Nonlinear Vibratory Energy Exchanges between a Two-Degree-of-Freedom Pendulum and a Nonlinear Absorber. J. Eng. Mech. 145 (8), 04019058. http://dx.doi.org/10.1061/(ASCE)EM.1943-7889.0001620.

Hurel, G., Ture Savadkoohi, A., Lamarque, C.-H., 2019b. Passive control of a two degrees-of-freedom pendulum by a non-smooth absorber. Nonlinear Dyn. 98, 3025–3036. http://dx.doi.org/10.1007/s11071-019-04891-0.

Ioi, T., Ikeda, K., 1978. On the Dynamic Vibration Damped Absorber of the Vibration System. Bull. JSME 21 (151), 64–71. http://dx.doi.org/10.1299/jsme1958.21.64.

Kuether, R., Renson, L., Detroux, T., Grappasonni, C., Kerschen, G., Allen, M., 2015. Nonlinear normal modes, modal interactions and isolated resonance curves. J. Sound Vib. 351, 299–310. http://dx.doi.org/10.1016/j.jsv.2015.04.035.

Lamarque, C.-H., Gendelman, O., Ture Savadkoohi, A., Etcheverria, E., 2011. Targeted energy transfer in mechanical systems by means of non-smooth nonlinear energy sink. Acta Mech. 221, 175–200. http://dx.doi.org/10.1007/s00707-011-0492-0.

Leroux, L., Langlois, S., Ture Savadkoohi, A., 2023. Investigation of a nonlinear control of galloping with a linear beam with elastic boundary conditions. Int. J. Non-Linear Mech. 156, 104484. http://dx.doi.org/10.1016/j.ijnonlinmec.2023.104484.

Luongo, A., Zulli, D., 2012. Dynamic analysis of externally excited NES-controlled systems via a mixed Multiple Scale/Harmonic Balance algorithm. Nonlinear Dynam. 70, 2049–2061. http://dx.doi.org/10.1007/s11071-012-0597-6.

Luongo, A., Zulli, D., 2014. Aeroelastic instability analysis of NES-controlled systems via a mixed multiple scale/harmonic balance method. J. Vib. Control 20 (13), 1985–1998. http://dx.doi.org/10.1177/1077546313480542.

Luongo, A., Zulli, D., 2015. Nonlinear energy sink to control elastic strings: the internal resonance case. Nonlinear Dynam. 81, 425–435. http://dx.doi.org/10.1007/s11071-015-2002-8.

Manevitch, L., 2001. The Description of Localized Normal Modes in a Chain of Nonlinear Coupled Oscillators using Complex Variables. Nonlinear Dynam. 25, 95–109. http://dx.doi.org/10.1023/A:1012994430793.

Nayfeh, A., Mook, D., 1995. Nonlinear Oscillations. John Wiley & Sons, New York.

Piccardo, G., Ranzi, G., Luongo, A., 2013. A complete dynamic approach to the Generalized Beam Theory cross-section analysis including extension and shear modes. Math. Mech. Solids 19 (8), 900–924. http://dx.doi.org/10.1177/1081286513493107.

Ranzi, G., Luongo, A., 2011. A new approach for thin-walled member analysis in the framework of GBT. Thin-Walled Struct. 49 (11), 1404–1411. http://dx.doi.org/10.1016/j.tws.2011.06.008.

Roberson, R.E., 1952. Synthesis of a nonlinear dynamic vibration absorber. J. Franklin Inst. 254 (3), 205–220. http://dx.doi.org/10.1016/0016-0032(52)90457-2.

Saeed, A., Abdul Nasar, R., AL-Shudeifat, M., 2023. A review on nonlinear energy sinks: designs, analysis and applications of impact and rotary types. Nonlinear Dynam. 111, 1–37. http://dx.doi.org/10.1007/s11071-022-08094-y.

Schardt, R., 1966. Eine Erweiterung der Technischen Biegetheorie zur Berechnung prismatischer Faltwerke. Der Stahlbau 35, 161–171, (In German).

Schardt, R., 1994. Generalized beam theory—an adequate method for coupled stability problems. Thin-Walled Struct. 19 (2), 161–180. http://dx.doi.org/10.1016/0263-8231(94)90027-2.

Silvestre, N., Camotim, D., 2002. First-order generalised beam theory for arbitrary orthotropic materials. Thin-Walled Struct. 40 (9), 755–789. http://dx.doi.org/10.1016/S0263-8231(02)00025-3.

Silvestre, N., Camotim, D., 2003. Nonlinear Generalized Beam Theory for Cold-formed Steel Members. Int. J. Struct. Stab. Dyn. 3 (4), 461–490. http://dx.doi.org/10.1142/S0219455403001002.

Starosvetsky, Y., Gendelman, O., 2008. Strongly modulated response in forced 2DOF oscillatory system with essential mass and potential asymmetry. Physica D 237 (13), 1719–1733. http://dx.doi.org/10.1016/j.physd.2008.01.019.

Starosvetsky, Y., Gendelman, O., 2011. Response regimes in forced system with nonlinear energy sink: quasi-periodic and random forcing. Nonlinear Dynam. 64, 177–195. http://dx.doi.org/10.1007/s11071-010-9856-6.

Troger, H., Steindl, A., 1991. Nonlinear Stability and Bifurcation Theory. An Introduction for Engineers and Applied Scientists. Springer-Verlag/Wien, New York.

Ture Savadkoohi, A., Lamarque, C.-H., Weiss, M., Vaurigaud, B., Charlemagne, S., 2016. Analysis of the 1:1 resonant energy exchanges between coupled oscillators with rheologies. Nonlinear Dynam. 86 (4), 2145–2159. http://dx.doi.org/10.1007/s11071-016-2792-3.

Vakakis, A.F., Gendelman, O.V., Bergman, L.A., McFarland, D.M., Kerschen, G., Lee, Y.S., 2008. Nonlinear Targeted Energy Transfer in Mechanical and Structural Systems I & II. Springer, Germany.

Vaurigaud, B., Ture Savadkoohi, A., Lamarque, C.-H., 2011. Targeted energy transfer with parallel nonlinear energy sinks. Part I: Design theory and numerical results. Nonlinear Dynam. 66, 763–780. http://dx.doi.org/10.1007/s11071-011-9949-x.

Wang, A.-P., Fung, R.-F., Huang, S.-C., 2001. Dynamic analysis of a tall building with a tuned-mass-damper device subjected to earthquake excitations. J. Sound Vib. 244 (1), 123–136. http://dx.doi.org/10.1006/jsvi.2000.3480.

Wang, Y., Kang, H., Cong, Y., Guo, T., Zhu, W., 2023. Vibration suppression of a cable under harmonic excitation by a nonlinear energy sink. Commun. Nonlinear Sci. Numer. Simul. 117, 106988. http://dx.doi.org/10.1016/j.cnsns.2022.106988.

Yang, Y., Yau, J., Wu, Y., 2004. Vehicle–Bridge Interaction Dynamics. World Scientific.

Zhang, Y.-W., Hou, S., Zhang, Z., Zang, J., Ni, Z.-Y., Teng, Y.-Y., Chen, L.-Q., 2020. Nonlinear vibration absorption of laminated composite beams in complex environment. Nonlinear Dynam. 99, 2605–2622. http://dx.doi.org/10.1007/s11071-019-05442-3.

Zulli, D., Luongo, A., 2015. Non linear energy sink to control vibrations of an internally non resonant elastic string. Meccanica 50, 781–794. http://dx.doi.org/10.1007/s11012-014-0057-0.

Zulli, D., Luongo, A., 2016. Control of primary and subharmonic resonances of a Duffing oscillator via non-linear energy sink. Int. J. Non-Linear Mech. 80, 170–182. http://dx.doi.org/10.1016/j.ijnonlinmec.2015.08.014.